https://doi.org/10.5194/essd-2025-746
Preprint. Discussion started: 2 February 2026

Open Access Earth System Science Data Discussions

Next-generation Metop ASCAT Surface Soil Moisture datasets

Sebastian Hahn[1], Thomas Melzer[1], and Wolfgang Wagner[1]

[1]Department of Geodesy and Geoinformation, TU Wien, Wiedner Hauptstraße 8, 1040 Vienna, Austria

Correspondence: Sebastian Hahn (sebastian.hahn@geo.tuwien.ac.at)

Abstract. This article presents the next-generation of the Advanced Scatterometer (ASCAT) surface soil moisture (SSM) dataset, bringing the operational near real-time (NRT) product up to date with the historical offline data record. For years, the offline data record has benefited from successive algorithmic improvements while the NRT product has only received minor updates. This release now applies the latest soil moisture retrieval algorithm and consistent fixed-Earth grid to both data streams, creating a unified dataset and representing a major advancement for the ASCAT SSM NRT product. Furthermore, the standard 12.5 km sampling ASCAT SSM dataset is now complemented by a new high-resolution 6.25 km sampling ASCAT SSM product. This is achieved by customising the spatial resampling process of the ASCAT Level 1B full-resolution backscatter data. A new key development in the change detection algorithm for ASCAT SSM concerns the estimation of the dry and wet backscatter references. Specifically, a moving-window approach is now applied instead of the full time series to mitigate artificial trends caused by long-term land cover changes. Additionally, a new monthly subsurface scattering flag has been added to filter out unreliable SSM measurements where backscatter and soil moisture indicate an inverted relationship.

Quality control of the ASCAT SSM datasets is performed by using soil moisture estimates from Noah GLDAS-2.1 and the ESA CCI Passive Soil Moisture (SM) v09.1 product, as well as in-situ observations provided by the International Soil Moisture Network (ISMN). The validation results show that both ASCAT SSM datasets have a comparable performance in terms of the Pearson correlation coefficient (ASCAT SSM 6.25 km vs ESA CCI Passive SM: 17.9 % > 0.75 and 57.8 % > 0.5; ASCAT SSM 12.5 km vs ESA CCI Passiv SM: 19.6 % > 0.75 and 59.2 % > 0.5) and signal-to-noise ratio (SNR) derived using triple collocation analysis (ASCAT SSM 6.25 km SNR: 56.0% > 0 dB, 35.6 % > 3 dB, ASCAT SSM 12.5 km SNR: 58.1 % > 0 dB, 38.6 % > 3 dB,). The best performance can be found in regions with strong seasonal variability, including monsoonal, savanna, Mediterranean, and tropical wet-and-dry zones. A lower performance can be found in areas characterised by limited soil moisture variability (such as deserts), dense vegetation, pronounced topographic complexity, wetland areas, or higher latitudes (> 60° N) experiencing longer periods of frozen soil and snow cover.

The ASCAT SSM datasets are publicly available online https://doi.org/10.15770/EUM_SAF_H_0011 and
https://doi.org/10.15770/EUM_SAF_H_0012
H SAF (2025a, c), while ASCAT SSM NRT products are additionally distributed via the broadcasting system EUMETCast.

1 Introduction

Soil moisture information derived from C-band (5.255 GHz) backscatter measurements acquired by the Advanced Scatterometer (ASCAT) has found widespread use in geoscientific applications such as numerical weather prediction, rainfall estimation,

https://doi.org/10.5194/essd-2025-746
Preprint. Discussion started: 2 February 2026

flood forecasting and drought monitoring (Dharssi et al., 2011; Draper et al., 2011; Gómez et al., 2020; Aires et al., 2021; Wanders et al., 2014; Brocca et al., 2012, 2014, 2017; Gaona et al., 2025). From the standpoint of the end-user, key advantages of ASCAT surface soil moisture (SSM) data include its operational availability, near-global daily coverage, and the provision of a long-term data record (Wagner et al., 2013). The latter is particularly crucial for studies related to climate change and applications that require consistent historical time series, either for enhancing process understanding or for the calibration of geophysical models. A prominent example is the ESA Climate Change Initiative (CCI) for soil moisture, which incorporates ASCAT SSM data as a core component within its active microwave soil moisture product (Dorigo et al., 2017; Gruber et al., 2019). Furthermore, ASCAT SSM data plays a key role in the operational product suites of both the Copernicus Climate Change Service (C3S) (Copernicus Climate Change Service, 2018) and Copernicus Land Monitoring Service (CLMS) (Bauer-Marschallinger et al., 2018).

In recent years, research on ASCAT soil moisture retrieval has made significant advances focusing on several key areas. These include the dynamic characterisation of the backscatter-incidence angle relationship (Melzer, 2013; Hahn et al., 2017; Vreugdenhil et al., 2017; Steele-Dunne et al., 2019, 2021), spatially-variable vegetation correction (Hahn et al., 2021), and the investigation and modelling of subsurface scattering effects (Morrison and Wagner, 2020; Wagner et al., 2022, 2024). Despite the progress in the dynamic characterisation of the incidence angle dependency of backscatter, a multi-year climatology is still being used in the operational processing chain. This is primarily due to the robustness and near real-time (NRT) suitability. In contrast, the spatially-variable vegetation correction has been successfully integrated and is now used on a regular basis. The study of subsurface scattering effects has provided insights into regions exhibiting an inverse relationship between backscatter and soil moisture. Various statistical and physically-based indicators have been developed to identify these regions, although a global implementation of the newly developed backscatter model remains to be realised. As an interim measure, a monthly subsurface scattering probability flag is now provided as a quality indicator to mask data from affected time periods (Lindorfer et al., 2023).

Table 1. Coarse resolution soil moisture datasets based on a single instrument.

Name	Sampling	Resolution	Availability	Reference
ASCAT SSM NRT 6.25 km	6.25 km	15 km	June 2025 - present	H SAF (2025b)
ASCAT SSM CDR + ICDR v1 6.25 km	6.25 km	15 km	Jan 2007 - present	H SAF (2025a)
ASCAT SSM NRT v2 12.5 km	12.5 km	25 km	June 2025 - present	H SAF (2025d)
ASCAT SSM CDR + ICDR v8 12.5 km	12.5 km	25 km	Jan 2007 - present	H SAF (2025c)
SMOS L2 SM V700	15 km	35-50 km	Jan 2010 - present	European Space Agency (2021)
SMOS NRT L2	15 km	35-50 km	Jan 2015 - present	Rodríguez-Fernández et al. (2017)
SMAP L2 SM, Version 9	36 km	36 km	Mar 2015 - present	ONeill et al. (2023a); Chan et al. (2016)
SMAP Enhanced L2 SM, Version 6	9 km	36 km	Mar 2015 - present	ONeill et al. (2023b); Chan et al. (2018)
LPRM AMSR-E	25 km	44-70 km	Jul 2002 - Oct 2011	Owe et al. (2008)

Relative to other (single sensor) remote sensing soil moisture products (see Table 1), ASCAT SSM strikes with a solid balance between retrieval accuracy and robustness across diverse environmental conditions. While NASA's Soil Moisture Active Passive (SMAP) mission usually performs best overall in validation studies, ESA's Soil Moisture and Ocean Salinity (SMOS) mission and ASCAT SSM are more closely matched, with either holding a slight edge depending on the regional environment or validation methodology (Al-Yaari et al., 2019; Beck et al., 2021; Fan et al., 2022; Kim et al., 2023; Xie et al., 2024). ASCAT SSM excels by providing a stable long-term record, capturing short-term dynamics effectively and its operational availability. Unlike SMAP and SMOS, which offer absolute soil moisture, ASCAT delivers relative values. This gives users the advantage of applying their own scaling or using their own soil maps to fit their specific needs. Consequently, it is important to understand that reported metrics such as root mean square difference (RMSD) and bias are linked to the selected conversion approach. Therefore, ASCAT's performance is often evaluated by its dynamic consistency, using scaling-insensitive metrics like temporal correlation and triple collocation analysis (TCA). A more comprehensive assessment of its value, however, comes from indirect applications such as generating rainfall estimates (SM2Rain) (Brocca et al., 2013, 2019; Kim et al., 2025) or quantifying the improvement in forecast skill achieved through data assimilation (Brocca et al., 2010; Draper et al., 2012; Seo et al., 2021).

In this article we present the latest ASCAT SSM data release, which for the first time includes a new high-resolution (6.25 km spatial sampling) dataset alongside the standard 12.5 km spatial sampling version. The theoretical spatial resolution for the new high-resolution dataset is 15 km, defined by the full width at half maximum (FWHM) of the spatial filter. However, the actual effective resolution varies depending on factors such as the number and size of the full-resolution backscatter observations used in the spatial resampling process. Furthermore, both ASCAT SSM datasets cover the period from January 2007 to December 2024. Over this time, long-term land cover changes have begun to noticeably affect the underlying backscatter observations, requiring correction to avoid artificial trends in the soil moisture retrievals. For this reason, a new moving-window calibration approach has been introduced to dynamically correct the backscatter signal and prevent non-hydrological long-term trends. In addition, the lower and upper bounds of the backscatter signal are now defined using percentile estimates to improve robustness and better represent local signal variability. As a consequence, the scaling range has been reduced from 0–100 % to 5–95 % to minimise the likelihood of observations saturating at the dry or wet (percentile) backscatter limits. The performance of both ASCAT SSM datasets is evaluated using in-situ observations from the International Soil Moisture Network (ISMN), satellite-based reference data from the ESA CCI Passive Soil Moisture product, and model-based soil moisture from NASA's Global Land Data Assimilation System (GLDAS).

2 Data

2.1 ASCAT Level 1B Sigma Zero Full-Resolution (SZF)

The Advanced Scatterometer (ASCAT) is a C-band (5.255 GHz) radar instrument designed to measure the Earth's surface backscatter coefficient, known as the Normalized Radar Cross Section (NRCS) or σ^0 expressed in $m^2\,m^{-2}$ or dB (Gelsthorpe et al., 2000; Figa-Saldana et al., 2002). At present, ASCAT backscatter measurements are currently acquired operational on-

https://doi.org/10.5194/essd-2025-746
Preprint. Discussion started: 2 February 2026

board the Metop-B and Metop-C satellites. The first satellite in the Metop series (Metop-A) also carried an ASCAT instrument and operated for 15 years before completing its mission in November 2021. The data collected by ASCAT are processed and distributed by the European Organization for the Exploitation of Meteorological Satellites (EUMETSAT) in several product formats.

EUMETSAT provides three types of ASCAT Level 1B backscatter products: Sigma Zero Full-Resolution (SZF), Sigma Zero Research (SZR) and Sigma Zero Operational (SZO). The ASCAT Level 1B SZR and SZO products represent spatially averaged backscatter values provided on orbit grid nodes with a sampling of 12.5 km (SZR) and 25 km (SZO). The ASCAT Level 1B SZF product corresponds to geo-located backscatter values along the six ASCAT beams, which are not collocated and spatially averaged on regular orbit grid nodes. Instead, 192 backscatter observations along every antenna beam projection on the ground are provided. The resolution of each backscatter "echo" varies slightly along the beam, measuring approximately 10 km in the along-beam direction and 25 km in the across-beam direction (Anderson et al., 2012).

The ASCAT Level 1B SZF backscatter product serves as the primary input for generating the ASCAT surface soil moisture (SSM) datasets. The backscatter measurements are first spatially resampled onto a fixed Earth grid (see Sect. 3.1), after which time series are constructed (see Sect. 3.2). As part of the change detection algorithm, model parameters are empirically estimated and applied to derive the ASCAT SSM datasets at two different spatial resolutions (see Sect. 3.3). Table 2 summarizes the observation periods of the ASCAT Level 1B SZF backscatter products for each Metop satellite.

Table 2. Observation periods of ASCAT Level 1B SZF data for each Metop satellite.

Satellite	Time period
Metop-A	2007-01-01 – 2021-11-15
Metop-B	2013-06-01 – 2024-12-31
Metop-C	2019-04-01 – 2024-12-31

2.2 ERA5

ERA5 is the fifth generation of the European Centre for Medium-Range Weather Forecasts (ECMWF) reanalysis dataset available from 1940 onward. The reanalysis combines model data with observations from across the world, providing a high-resolution, globally consistent representation of land, ocean, and atmospheric conditions. In this study, we used hourly soil temperature level 1 (stl1) and snow depth (sd) data to identify and exclude periods with frozen soil or snow cover when estimating dry and wet backscatter references (see Sect. 3.3.5). Additionally, these variables were used to generate a frozen soil and snow cover probability flag based on 40 years of data (see Sect.s 3.4.3 and 3.4.4). Finally, the same ERA5 variables were also utilized during validation to identify ASCAT SSM observations affected by frozen soil or snow cover (see Sect. 3.5).

https://doi.org/10.5194/essd-2025-746
Preprint. Discussion started: 2 February 2026

2.3 Noah GLDAS-2.1

The Global Land Data Assimilation System Version 2.1 (GLDAS-2.1) is a state-of-the-art land surface modeling system designed to provide high-resolution global land surface states, including soil moisture, soil temperature, and energy fluxes (Rodell et al., 2004; Beaudoing et al., 2020). One of the primary models used in GLDAS-2.1 is the Noah Land Surface Model (Noah LSM), which provides a physically based representation of soil moisture dynamics by simulating four soil layers at depths of 0–10 cm, 10–40 cm, 40–100 cm, and 100–200 cm. The soil moisture data are provided in $\mathrm{kg\,m^{-2}}$, three-hourly (00:00, 03:00, 06:00, 09:00, 12:00, 15:00, 18:00, and 21:00 UTC) and monthly averages at a spatial sampling of 0.25° (~25 km), making it suitable for global and regional hydrological assessments. In this study, we used soil moisture information from the first layer (0–10 cm) of the three-hourly GLDAS-2.1 product as an independent reference dataset for validating the ASCAT SSM datasets (see Sect. 3.5).

2.4 ESA CCI Passive Soil Moisture

The ESA CCI Passive Soil Moisture (SM) v09.1 product is a global dataset developed by the European Space Agency's Climate Change Initiative (ESA CCI), designed to provide consistent long-term soil moisture information based on passive microwave remote sensing observations from Nimbus 7 SMMR, DMSP SSM/I, TRMM TMI, Aqua AMSR-E, Coriolis WindSat, GCOM-W1 AMSR2, SMOS and SMAP (Dorigo et al., 2017; Gruber et al., 2019). The ESA CCI Passive SM v09.1 product covers the period from 1978 to 2023, with a spatial sampling of 0.25° (~25 km) and a daily temporal resolution, expressed in volumetric soil moisture units ($\mathrm{m^3\,m^{-3}}$). The ESA CCI Passive SM v09.1 product is used as an independent reference for validating the ASCAT SSM datasets (see Sect. 3.5).

2.5 ESA CCI Land Cover

The ESA CCI Land Cover (LC) dataset provides global land cover maps from 1992 to 2022 at a spatial resolution of 300 m (ESA, 2017). Version 2.0.7 covers the period 1992–2015, while version 2.1.1 extends the record from 2016 onwards. Both versions are produced using the same processing chain to ensure temporal consistency across the entire dataset. Each annual map is generated by detecting land cover changes relative to a unique baseline LC map, which is derived from the Medium Resolution Imaging Spectrometer (MERIS) Full Resolution (FR) and Reduced Resolution (RR) archive covering 2003–2012.

The ESA CCI LC map for 2018 is used to generate a fractional LC dataset, spatially aligned with the resolution of ASCAT backscatter measurements. This dataset is used to identify and exclude unwanted backscatter signals originating from lakes, urban areas, and open water (see Sect. 3.1).

2.6 Global Lakes and Wetlands Database (GLWD)

The Global Lakes and Wetlands Database (GLWD) represents a combination of existing data sources for lakes and wetlands on a global scale (Lehner and Döll, 2004). The database focuses on three level: (i) large lakes and reservoirs, (ii) smaller water bodies and (iii) wetlands. In this study, the GLWD dataset is used to calculate the wetland fraction flag (see Sect. 3.4.1).

https://doi.org/10.5194/essd-2025-746
Preprint. Discussion started: 2 February 2026

2.7 Copernicus DEM

The Copernicus Digital Elevation Model (Copernicus DEM) is a global Digital Surface Model (DSM) that represents the elevation of the Earth's surface, including natural terrain features and built structures (Copernicus, 2021). It is derived from data acquired by the TanDEM-X satellite mission between 2011 and 2015. In this study, the 90 m spatial resolution version of the Copernicus DEM (GLO-90) is used for the calculation of the topographic complexity flag (see Sect. 3.4.2).

2.8 Global Subsurface Scattering Maps

Wagner et al. (2024) developed global maps that identify areas influenced by subsurface scattering, using both statistical analyses and physically-based indicators (Lindorfer et al., 2023). Subsurface scattering can induce an inverse relationship between backscatter and soil moisture, thereby compromising the interpretation of backscatter variations in the ASCAT soil moisture change detection algorithm. Although a recently developed backscatter model, which includes a subsurface scattering term, successfully explained backscatter anomalies in arid environments (Wagner et al., 2022), its implementation at the global scale is still pending. Consequently, the ASCAT SSM datasets must be masked for spatial and temporal subsurface scattering effects. A monthly probability of backscatter anomalies from Wagner et al. (2024) is provided as part of the ASCAT SSM datasets and applied during validation (see Sect. 3.5).

2.9 In-situ data

The International Soil Moisture Network (ISMN) serves as a data portal that maintains global in-situ soil moisture observations (Dorigo et al., 2011, 2021). A collaborative effort among various network operators helps to collect and maintain in-situ data worldwide. The primary objective of the ISMN soil moisture database is to provide ground reference data for the validation of satellite soil moisture products. In this study, we selected a total number of 44 in-situ networks containing sensors with a depth range of 0–10 cm. The list of ISMN networks can be found in Table A1. The spatial and temporal extent of these networks is variable, as well as their land cover and climate characteristics. Smaller networks with less stations represent very local conditions (e.g. DAHRA,, IIT_KANPUR, LAB-net, LABLUX, SKKU, VAS), while larger networks cover a number of different climate zones and land cover classes (e.g. SCAN, SNOTEL, USCRN).

3 Methodology

The ASCAT Surface Soil Moisture (SSM) datasets are generated using a physically-based change detection approach, which was initially developed for backscatter observations from ERS-1/-2 (Wagner et al., 1999a, b, c; Scipal et al., 2002). This method takes advantage of the strong dependency of the radar backscatter intensity to variations in soil moisture content. As soil moisture increases, the dielectric constant at the air-soil interface also rises, resulting in a stronger backscatter signal (Wagner et al., 2013). However, recent research has also shown that under special circumstances subsurface scattering can induce an

https://doi.org/10.5194/essd-2025-746
Preprint. Discussion started: 2 February 2026

inverse relationship, most notably in arid environments with strong scatters beneath shallow soil (Wagner et al., 2022, 2024). Therefore, an accurate quantification and mitigation of such subsurface scattering effects has become a major focus of research.

The change detection algorithm relies on calibrated model parameters, which are independently estimated for each location using historical backscatter observations. Therefore, as part of the pre-processing procedure, a time series of backscatter observations is generated from spatially resampled ASCAT Level 1B Sigma0 Zero Full-Resolution (SZF) swath data. The semi-empirical model parameters are needed to model and correct azimuth and incidence angle effects and to scale normalised backscatter observations between dry and wet backscatter references. The resulting soil moisture estimates are expressed in degree of saturation, ranging from 0 % (dry) to 100 % (saturated soil) representing the topsoil layer (< 5 cm).

It is important to note that, the generation of the backscatter time series and the estimation of semi-empirical model parameters are carried out offline. By computing all necessary parameters in advance, the soil moisture retrieval can be efficiently performed on the original ASCAT Level 1B Sigma0 Zero Full-Resolution (SZF) swath data. This setup also allows a near real-time (NRT) application of the change detection method. Figure 1 provides an overview of the entire workflow, with each step described in more detail in the following subsections.

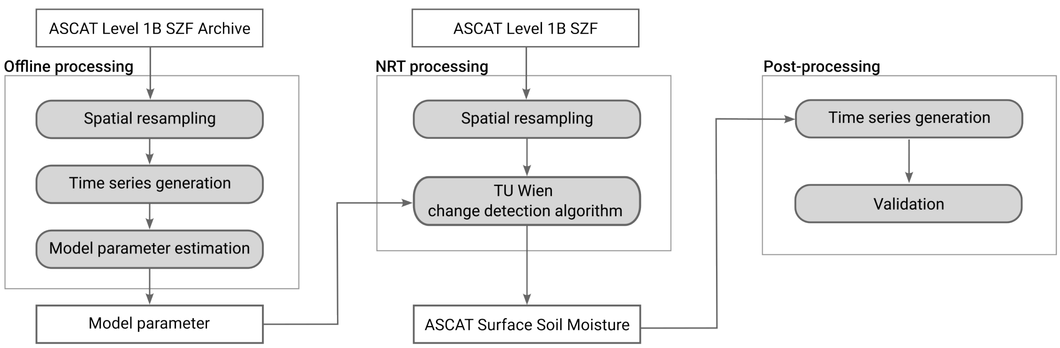

Figure 1. Processing workflow showing (i) the estimation of the semi-empirical model parameter, (ii) the retrieval of surface soil moisture using the TU Wien change detection algorithm, and (iii) validation as part of the post-processing.

3.1 Spatial resampling

3.1.1 Aggregation and filtering

The ASCAT Level 1B Sigma Zero Full-resolution (SZF) dataset contains backscatter observations σ^0 (also called "echos") at very high spatial resolution for each antenna beam (Fore, Mid, Aft), which are spatially not perfectly collocated. The spatial extent, shape, and orientation of an individual echo is determined by the observation geometry, on-board processing in range and Doppler frequency. The spatial response function (SRF) is used to describe how the backscatter signal is weighted across the surface footprint (Lindsley et al., 2016; Vogelzang et al., 2017).

https://doi.org/10.5194/essd-2025-746
Preprint. Discussion started: 2 February 2026

Open Access Earth System Science Data Discussions

The spatial resampling process aims to generate consistent backscatter triplets at a coarser spatial resolution by filtering and aggregating echos from individual beams, thereby also reducing inherent observational noise. The spatial extent and resolution is given by its cumulative spatial response function (CSRF) determined by the window function and its associated spatial radius applied during the aggregation of the echos. Backscatter is first converted from the decibel scale to the linear domain, where a weighted average is computed. The averaged backscatter is then converted back to the decibel scale. A weighted average is also applied to the incidence and azimuth angles, providing a consistent representation of the observation geometry. In addition, the normalized noise variance (known as kp-value) is also derived for the averaged backscatter, representing the relative standard deviation of the noise within the averaging area (see Equation 1). The kp-value not only reflects natural surface heterogeneity but also noise contributions, such as those affected by radiometric resolution.

$$\mathrm{kp} = \frac{\mathrm{StdDev}\left[\sigma^0\right]}{\mathrm{Mean}\left[\sigma^0\right]} \tag{1}$$

A Hamming window (see Equation 2) with a spatial radius (X) of approximately 14 km is applied to generate backscatter triplets sampled at a grid spacing of 6.25 km, yielding a theoretical spatial resolution of 15 km. This theoretical resolution is defined by the full width at half maximum (FWHM) of the spatial filter (Figa-Saldana et al., 2002). The actual spatial resolution, however, cannot be determined precisely since it varies depending on factors such as the number and size of the full-resolution backscatter observations used in the spatial resampling process. Unlike the ASCAT Level 1B SZR and SZO datasets provided by EUMETSAT, which are sampled on orbit-specific grid nodes, the backscatter triplets are located on a fixed Earth grid. This approach allows the resampled ASCAT Level 1B SZF backscatter data to be easily stacked, enabling the construction of a time series during subsequent processing.

$$w\left(x\right) = 0.54 - 0.46\cos\left(2\pi\frac{x}{X}\right), 0 \leq x \leq X \tag{2}$$

Additionally, a second backscatter triplet dataset is also generated at a coarser grid spacing of 12.5 km, using a spatial radius of 24 km, resulting in a theoretical spatial resolution of 25 km. Both backscatter triplet datasets are independently used to produce two ASCAT surface soil moisture (SSM) datasets, sampled at 6.25 km and 12.5 km, respectively. The 12.5 km sampling corresponds to the standard spatial sampling distance also used by the ASCAT Level 1B SZR product, whereas the 6.25 km dataset is designed to maximise spatial detail while retaining an acceptable noise level.

Not all backscatter echos are included in the aggregation process. Echos located over areas not sensitive to soil moisture changes (open water, coastal regions, urban areas) are excluded. The identification of these echos is achieved using the ESA CCI Land Cover dataset (v2.1.1), which is pre-processed to represent a fractional land cover dataset, aligned with the spatial resolution of the backscatter echos. This way, unwanted backscatter observation are determined and filtered. In addition, an outlier detection method based on the Median Absolute Deviation (MAD) is applied to further refine the spatially resampled dataset by removing echos that deviate significantly from the expected behaviour ($\sigma^0 > 3 \times \mathrm{MAD}$), ensuring the reliability of the aggregated backscatter data.

https://doi.org/10.5194/essd-2025-746
Preprint. Discussion started: 2 February 2026

Open Access Earth System Science Data Discussions

$$\mathrm{MAD} = \mathrm{median}\left(\left|\sigma_i^0 - \mathrm{median}(\sigma^0)\right|\right) \tag{3}$$

It should be emphasised that the ASCAT Level 1B SZF dataset is spatially resampled into 60-minute segments to avoid any ambiguity caused by a spatial overlap. To ensure complete sampling of the swath edges, a temporal buffer is added at both the beginning and end of each segment ($\pm$ 5 minutes), allowing all relevant echos to be included. In a near real-time processing scenario, the segments are much smaller ($\approx$ 3 minutes), but a temporal buffer is still needed to include all relevant backscatter observations.

3.1.2 Fibonacci grid

The Fibonacci grid was selected as the fixed Earth reference grid. It is designed to uniformly distribute points across the surface of a sphere. Inspired by the Fibonacci sequence and the golden ratio ($\phi = 1 + \phi^{-1} = \left(1+\sqrt{5}\right)/2 \approx 1.618$), it ensures a nearly equal-area distribution of points. Constructing the grid involves distributing points along the vertical axis of the sphere (latitude) and rotating them around the sphere's horizontal axis (longitude) based on the complementary golden angle ($360°\phi^{-1} \approx 222.5°$). This deterministic approach is computationally efficient and scales easily by adjusting the number of points. Unlike traditional latitude-longitude grids (e.g. 1°× 1°), the Fibonacci grid systematically spaces points to avoid clustering at the poles. The Fibonacci grid points, initially calculated on a sphere, are transformed into ellipsoidal coordinates to align with the coordinate reference system used to geo-locate ASCAT backscatter data (WGS84). However, this transformation alters distances between points on a larger scale due to differences in curvature between the sphere and the ellipsoid. Fortunately, only short distances (< 25 km) are relevant for the resampling process, minimising the impact of the coordinate transformation.

The Fibonacci grid is generated using the following formulas (Álvaro González, 2009). The absolute number of points P is defined by a natural number N, which is the only parameter to be determined to generate a Fibonacci grid.

$$P = 2N + 1 \tag{4}$$

The spherical coordinates (expressed in radians) of the ith point are

$$\mathrm{lat}_i = \arcsin\left(\frac{2i}{2N+1}\right), \quad i = -N, \ldots, N \tag{5}$$

$$\mathrm{lon}_i = 2\pi i \phi^{-1}, \quad i = -N, \ldots, N \tag{6}$$

The Fibonacci grid representing an approximate sampling of 6.25 km is composed of 13,200,001 points (N=6,600,000), whereas the approximate sampling of 12.5 km is realised by 3,300,001 points (N=1,650,000). In both cases, only one-third of the grid points are situated over land surfaces. An example of the 12.5 km Fibonacci grid is shown in Figure 2.

https://doi.org/10.5194/essd-2025-746
Preprint. Discussion started: 2 February 2026

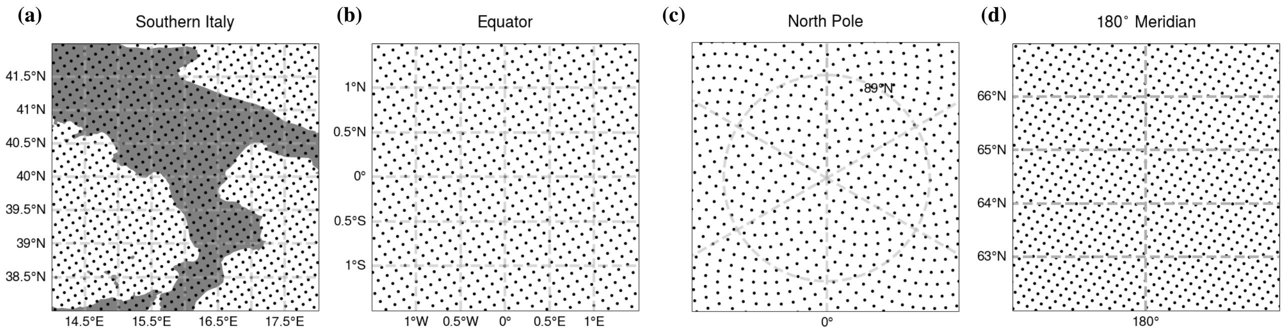

Figure 2. Fibonacci grid with 12.5 km sampling is shown for (a) Southern Italy, (b) the Equator, (c) the North Pole, and (d) the 180° meridian.

3.2 Backscatter time series generation

The resampled backscatter swath segments are stored according to the Climate and Forecast (CF) point data model (Eaton et al., 2024), which standardises the representation of individual geo-referenced observations. In the next step, the point data are systematically transformed into the CF index ragged array format, a data structure tailored for time series representation. In this new format, all point observations are consolidated into a single array, while an index variable links each observation to its corresponding location on the fixed Earth grid. This approach facilitates a flexible and scalable storage of time series data for each grid location. Furthermore, the data format supports integrating any future observations, allowing a seamless extension of the time series. Optionally, the final time series can be converted into the CF contiguous ragged array format, which optimises data access performance by ensuring a chronological sorting for each grid location. However, this format compromises the ease of future data extension due its strict sorting structure.

3.3 TU Wien change detection algorithm and model parameter estimation

The semi-empirical change detection method has been developed by the Vienna University of Technology (TU Wien) and was initially applied to backscatter observations acquired by the Advanced Microwave Instrument (AMI) on-board the ERS-1 and ERS-2 satellites (Wagner et al., 1999a, b, c; Scipal et al., 2002). Thanks to a similar instrument design, the same methodology was later successfully adapted for the Advanced Scatterometer (ASCAT) on-board the series of Metop satellites (Bartalis et al., 2006b, 2007; Naeimi et al., 2009a, b). The change detection method eliminates the need for explicit surface roughness parameterisation and leverages multi-incidence angle backscatter observations to simultaneously model soil moisture and vegetation dynamics (Wagner et al., 2013). From a mathematical perspective, the change detection method is simpler than a radiative transfer model and can be solved directly without the need for a non-linear iterative optimisation.

The backscatter triplet dataset in time series format serves as input for the model parameter estimation procedure. Backscatter varies primarily due to surface dielectric properties, roughness, and vegetation, which are the most influential factors. Additionally, its overall magnitude is strongly affected by the measurement geometry, i.e. the incidence angle (θ) and the az-

https://doi.org/10.5194/essd-2025-746
Preprint. Discussion started: 2 February 2026

imuth angle (ϕ). To accurately attribute backscatter variations to changes in soil moisture, both the azimuth and incidence angle dependencies of backscatter must be addressed.

3.3.1 Azimuth angle dependency of backscatter

Azimuth angle dependency of backscatter is very common over land and can be particularly pronounced in mountainous areas or sandy deserts (Stephen and Long, 2002). The anisotropic nature of a target is closely related to the satellite's orbit and the instrument's geometry. A backscatter signal bias caused by azimuthal modulation can significantly affect the retrieval of geophysical parameters, such as soil moisture.

Similar to Bartalis et al. (2006a), an empirical approach is used to derive statistically expected values for a combination of observation geometries, which in the end normalises σ^0 observations with respect to the azimuth angle. The azimuth angle is determined by the beam (Fore, Mid, or Aft), the swath position (left or right), and the orbit direction (ascending or descending), resulting in twelve distinct azimuth configurations (ϕ_i, where $i \in [1,12]$) for ASCAT. For each azimuth configuration, the dependency of backscatter on the incidence angle is modelled using a second-order polynomial estimating the coefficients a_i, b_i, c_i.

$$\sigma_i^0(\theta) = a_i(\theta - 40)^2 + b_i(\theta - 40) + c_i \tag{7}$$

Additionally, a reference model ($i = 13$) is fitted to all observations combined. This results in a total of 3 × 13 = 39 coefficients. The differences between the polynomial coefficients of the twelve individual acquisition geometries and the reference model ($i = 13$) are used to derive new polynomial coefficients, which are then used to compute corrections applied to the backscatter observation. In this way, the individual observation configuration are adjusted to a common reference, effectively eliminating static azimuth angle effects.

$$\begin{aligned}\hat{\sigma}_i^0(\theta) = \sigma_i^0(\theta) - ((a_{13} - a_i)(\theta - 40)^2 \\ + (b_{13} - b_i)(\theta - 40) + (c_{13} - c_i))\end{aligned} \tag{8}$$

where $\hat{\sigma}_i^0$ represents the corrected backscatter for each configuration i.

3.3.2 Estimated standard deviation of backscatter

The Estimated Standard Deviation (ESD) quantifies the standard deviation of backscatter (expressed in dB) and serves as a measure of noise. Computing the ESD represents the initial step in error propagation. It is derived from the Fore and Aft beam measurements (σ_f^0, σ_a^0) based on the following assumption: all three beams observe the same target, and the Fore and Aft beams share identical incidence angles due to the instrument observation geometry. Consequently, in the absence of azimuth angle dependency of backscatter, the measurements from the Fore and Aft beams should be comparable, meaning they are statistically instances of the same distribution. Therefore, the expected value of their difference

https://doi.org/10.5194/essd-2025-746
Preprint. Discussion started: 2 February 2026

$$\delta := \mathrm{E}\left[\sigma_f^0 - \sigma_a^0\right] = 0 \quad (9)$$

295 should be zero, and its variance should be twice the variance of one of the beams (i.e $\mathrm{Var}[\delta] = 2\mathrm{Var}\left[\sigma^0\right]$). This can be derived using error propagation and neglecting higher order terms. Hence, the ESD is defined as

$$\mathrm{ESD}\left[\sigma^0\right] \approx \sqrt{\frac{\mathrm{Var}[\delta]}{2}} \quad (10)$$

3.3.3 Incidence angle dependency of backscatter

Over land surfaces, backscatter generally decreases with increasing incidence angle, a relationship that is often approximated by a linear function in the decibel (dB) domain. However, at larger incidence angles, significant contributions from volume scattering can cause the backscatter signal to increase, leading to deviations from the linear relationship (see Figure 3) (Wagner et al., 2013). To account for these higher-order variations, a second-order function provides a more accurate representation of the incidence angle dependence. A well-calibrated model of the incidence angle dependence of backscatter has two key objectives. First, it allows interpolating backscatter observations across different incidence angles, e.g. interpolating all observations to a common reference incidence angle. Second, changes of the incidence angle behaviour can reveal valuable information about surface characteristics and underlying geophysical parameters.

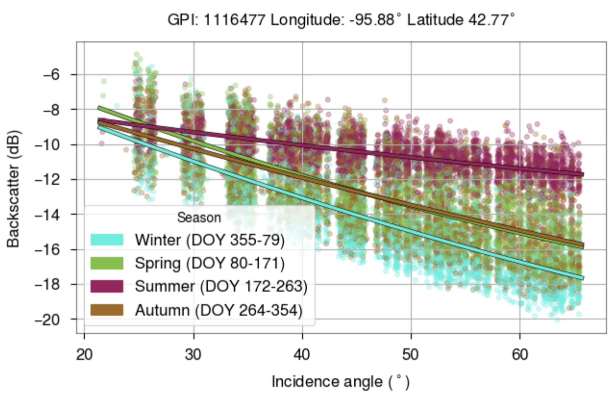

Figure 3. Backscatter variation with incidence angle over agricultural land in northwest Iowa, USA.

In this case, a second-order Taylor polynomial is used to model the incidence angle dependence of backscatter. The model represents a finite sum of the function's first and second derivative with the incidence angle of 40° serving as the expansion point.

310 $$\sigma^0(\theta) = \sigma^0(40) + \sigma'(\theta - 40) + \frac{1}{2}\sigma''(\theta - 40)^2 \quad (11)$$

https://doi.org/10.5194/essd-2025-746
Preprint. Discussion started: 2 February 2026

The first derivative, σ' (dB degree^{-1}), and the second derivative, σ'' (dB degree^{-2}), are referred to as the slope and curvature, respectively. Once these parameters are estimated, the Taylor polynomial expansion can be used to approximate the backscatter in the vicinity of the chosen expansion point. This approach allows for the interpolation of backscatter observations from their original incidence angles to a common reference incidence angle. At the reference incidence angle, backscatter observations can be directly compared, as the dependency on incidence angle has been effectively eliminated.

$$\sigma'_{fm} = \frac{\sigma^0_m - \sigma^0_f}{\theta_m - \theta_f}, \quad \sigma'_{am} = \frac{\sigma^0_m - \sigma^0_a}{\theta_m - \theta_a} \tag{12}$$

The estimation of σ' and σ'' is based on the computation of the local slope (see Equation 12), which provides an instantaneous characterisation of the incidence angle dependence of the backscatter signal. Since the Mid beam incidence angle is separated by approximately 9° compared to the Fore and Aft beam incidence angle, two local slope values can be obtained from a backscatter triplet. Typically a larger number of Fore-Mid and Aft-Mid beam observations are required to capture a sufficiently wide range of incidence angles. Ultimately, σ' and σ'' are estimated through a weighted local linear regression performed for each day of the year (Melzer, 2013). A detailed description of the methodology can be found in Hahn et al. (2017). It is based on a Kernel Smoother (KS) approach using the Epanechnikov kernel to weigh observations based on their temporal distance from the target day. A kernel bandwidth of $\lambda = 21$ days is used, which corresponds to a symmetric smoothing window of 42 days.

Depending on the number of years included in the computation, the estimates of σ' and σ'' may represent either a multi-year climatology or a year-specific time series. Although a year-specific time series would allow for the assessment of inter-annual variability, a multi-year climatology is currently used to ensure greater robustness and suitability for near real-time applications (Steele-Dunne et al., 2019, 2021).

3.3.4 Interpolation to reference incidence angle

The slope and curvature parameters are calculated for each day of the year (d) and used in the Taylor polynomial to interpolate backscatter observations to a common reference incidence angle of 40°. This angle is selected to be close to the centre of the observed incidence angle range to minimise interpolation errors. The interpolation is performed independently for each beam (b) (see Equation 13), and the resulting values are averaged across all three beams at 40° to further reduce noise (see Equation 14).

$$\sigma^0_b(40,t) = \sigma^0_b(\theta_b,t) - \sigma'(d(t)) \cdot \Delta\theta_b - \frac{1}{2} \cdot \sigma''(d(t)) \cdot \Delta\theta_b^2 \tag{13}$$

$$\bar{\sigma}^0(40,t) = \frac{1}{3} \cdot \sum_{b \in \{f,m,a\}} \sigma^0_b(40,t) \tag{14}$$

https://doi.org/10.5194/essd-2025-746
Preprint. Discussion started: 2 February 2026

3.3.5 Estimation of dry and wet backscatter reference

The dry and wet backscatter references represent the lower and upper bounds of backscatter associated with dry and wet soil conditions, respectively. These references are essential because they compensate for static (e.g. surface roughness) and dynamic influences (e.g. vegetation phenology) on the backscatter signal. By scaling backscatter observations to these bounds, signal variations should primarily reflect relative changes in soil moisture, minimising the impact of other effects. Furthermore, observations taken during periods of frozen soil and snow cover are excluded from the computation. Although frozen soil and dry soil have similarly low dielectric constants, in practice, backscatter values can decrease substantially under frozen conditions, making them unsuitable for defining the dry reference.

Traditionally, the dry and wet backscatter references have been estimated from the entire backscatter time series, which has proven effective over periods of 3 to 8 years. However, as the record now spans more than 15 years, long-term land cover changes have become a significant source of trends in backscatter, such as deforestation or urbanisation. Therefore, a monthly estimation approach using a moving window of ± 42 months (i.e. ± 3.5 years) has been implemented. This way, the dry and wet backscatter reference are able to gradually adapt to non-soil moisture related changes over time.

The lowest and highest backscatter values corresponding to dry and wet soil conditions are derived by interpolating the observed backscatter to specific incidence angles (see Equation 15 and 16). These angles, known as the dry and wet cross-over angles (θ_d, θ_w), are selected to minimise the influence of vegetation. The initial values were empirically set to $\theta_d = 25°$ and $\theta_w = 40°$ and applied globally (Wagner et al., 1999b, c, a). More recently, these parameters have been spatially parameterised to better account for seasonal vegetation effects (Hahn et al., 2021), and this updated approach has been applied.

$$\sigma^0(\theta_d,t) = \sigma^0(40,t) + \sigma'(d(t)) \cdot \Delta\theta_d + \frac{1}{2} \cdot \sigma''(d(t)) \cdot \Delta\theta_d^2 \tag{15}$$

$$\sigma^0(\theta_w,t) = \sigma^0(40,t) + \sigma'(d(t)) \cdot \Delta\theta_w + \frac{1}{2} \cdot \sigma''(d(t)) \cdot \Delta\theta_w^2 \tag{16}$$

with $\Delta\theta_d = (\theta_d - 40)$ and $\Delta\theta_w = (\theta_w - 40)$.

The selection of these specific angles is motivated by the so-called cross-over angle concept (Wagner et al., 1999a), according to which the backscatter-incidence angle curves for constant soil moisture and different vegetation states intersect at a characteristic angle where the effect of vegetation on the backscatter is minimised. By using these cross-over angles, it is possible to isolate soil moisture signals from vegetation influences and obtain reliable dry and wet references. At these angles, the lower (dry) and upper (wet) bounds of the backscatter distribution are derived using the 2nd and 98th percentiles computed within a ± 42-month moving window centred on each calendar month (see Equation 17 and 18). These values are subsequently converted back to the reference incidence angle, which also changes the temporal resolution from monthly to daily due to slope and curvature parameters (see Equation 19 and 20).

$$\sigma_d^0(\theta_d, m_j) = \mathrm{P}_2\left(\left\{\sigma_i^0 \mid m_j - 21 \leq \mathrm{month}(t_i) \leq m_j + 20\right\}\right) \tag{17}$$

https://doi.org/10.5194/essd-2025-746
Preprint. Discussion started: 2 February 2026

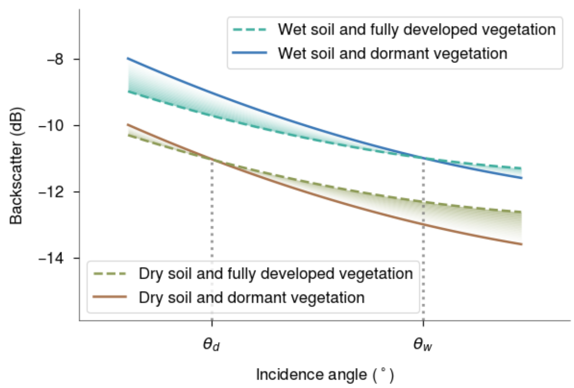

Figure 4. Cross over angle concept.

$$\sigma_w^0(\theta_w, m_j) = \mathrm{P}_{98}\left(\left\{\sigma_i^0 \,\middle|\, m_j - 21 \leq \mathrm{month}(t_i) \leq m_j + 20\right\}\right) \tag{18}$$

with m_j being the month of interest, $\mathrm{month}(t_i)$ the month of the observation time stamp, σ_i^0 measurements within the current time window and $\sigma_d^0(\theta_d)$ the dry reference at the dry cross-over angle. Similarly, the wet reference, $\sigma_w^0(\theta_w)$, is computed as the 98th percentile. The selection of these specific percentiles was empirically determined to provide stable and representative reference bounds.

$$\sigma_d^0(40, d) = \sigma_d^0(\theta_d, m(d)) - \sigma'(d) \cdot \Delta\theta_d - \frac{1}{2} \cdot \sigma''(d) \cdot \Delta\theta_d^2 \tag{19}$$

$$\sigma_w^0(40, d) = \sigma_w^0(\theta_w, m(d)) - \sigma'(d) \cdot \Delta\theta_w - \frac{1}{2} \cdot \sigma''(d) \cdot \Delta\theta_w^2 \tag{20}$$

It should be noted that the dry and wet backscatter references, as well as the slope and curvature parameters, are provided with daily time stamps and are converted to backscatter observation time stamps when required. If multiple backscatter observations occur on the same day, the corresponding reference values are assigned identically to each observation.

3.3.6 Wet correction

In some regions, truly saturated soil conditions are rarely or never observed due to prevailing climatic factors. Therefore, a correction must be applied to simulate wet conditions and obtain a more realistic wet reference. This wet correction relies on an external climate dataset (Peel et al., 2007), as scatterometer measurements alone are insufficient to reliably identify such regions. The correction is implemented in two steps: (i) first the lower limit of the wet reference is set to at least -10 dB and (ii) regions where saturated soil moisture conditions are rarely encountered (Köppen Geiger climate class B), $\sigma_w^0(40)$ values are raised until the sensitivity (defined as $\sigma_w^0(40) - \sigma_d^0(40)$) reaches a minimum of 5 dB (Naeimi et al., 2009b).

https://doi.org/10.5194/essd-2025-746
Preprint. Discussion started: 2 February 2026

Open Access Earth System Science Data Discussions

3.3.7 Soil moisture computation

Backscatter observations are scaled between the dry and wet references to yield relative soil moisture, expressed as degree of saturation from 0 % (dry soil) to 100 % (saturated soil). Notably, the dry and wet backscatter reference values reflect extreme conditions based on historical observations, and are derived using percentile estimation. To account for the associated uncertainty and variability, backscatter observations are scaled between 5 and 95 % saturation (i.e., $a = 5$, $b = 95$), as defined in Equation 21. This approach also aims to minimise the risk of mapping sequences of either low or high backscatter values to extreme soil moisture levels, as this can negatively impact e.g. drought indicators. Furthermore, mild outliers identified by soil moisture values in the intervals -20–0 % and 100–120 %, are set to 0 % and 100 %, respectively. Strong outliers, defined as less than -20 % or more than 120 are assigned a value of NaN.

$$m_s\left(t\right) = a + \frac{\sigma^0\left(40,t\right) - \sigma_d^0\left(40,d(t)\right)}{\sigma_w^0\left(40,d(t)\right) - \sigma_d^0\left(40,d(t)\right)} \cdot (b-a) \tag{21}$$

3.3.8 Error propagation

The Estimated Standard Deviation of backscatter (ESD$[\sigma^0]$) serves as the basis for error propagation. These backscatter uncertainties are carried forward to the variances of the estimated slope and curvature parameters (Var$[\sigma']$, Var$[\sigma'']$), which are derived under the assumption that all local slope values exhibit identical, uncorrelated variances, as described by Hahn et al. (2017). The variance of the local slopes is estimated from the residuals of the weighted local linear regression, which is performed using the Epanechnikov kernel. All of these error estimates are subsequently propagated to quantify the uncertainty of the backscatter values interpolated to the reference incidence angle of 40°:

$$\mathrm{Var}\left[\sigma_b^0\left(40,t\right)\right] = \mathrm{ESD}\left[\sigma^0\right]^2 + \mathrm{Var}\left[\sigma'\left(d(t)\right)\right] \cdot \Delta\theta_b^2 + \frac{1}{4} \cdot \mathrm{Var}\left[\sigma''\left(d(t)\right)\right] \cdot \Delta\theta_b^4 \tag{22}$$

Upon averaging for each beam, the noise variance becomes:

$$\mathrm{Var}\left[\bar{\sigma}^0\left(40,t\right)\right] = \frac{1}{9} \cdot \sum_{b\in\{f,m,a\}} \mathrm{Var}\left[\sigma_b^0\left(40,t\right)\right] \tag{23}$$

Although error propagation is applied when converting backscatter observations to the dry and wet cross-over angles, the resulting propagated errors are not directly used. This is because the dry and wet backscatter references are derived from percentiles of the backscatter distributions rather than from individual measurements. As a result, the associated variances (Var$[\sigma_d^0]$, Var$[\sigma_w^0]$) cannot be explicitly calculated through standard error propagation and are therefore not accounted for in this step. However, error propagation formulas are explicitly applied during the conversion of the dry and wet backscatter references to the common reference incidence angle of 40°. In this case, the total noise is computed using the following expressions:

https://doi.org/10.5194/essd-2025-746
Preprint. Discussion started: 2 February 2026

$$\mathrm{Var}\left[\sigma_d^0(40,d)\right] = \mathrm{Var}\left[\sigma_d^0(\theta_d, d(t))\right] + \mathrm{Var}\left[\sigma'(d(t))\right] \cdot \Delta\theta_d^2 + \frac{1}{4} \cdot \mathrm{Var}\left[\sigma''(d(t))\right] \cdot \Delta\theta_d^4 \tag{24}$$

$$\mathrm{Var}\left[\sigma_w^0(40,d)\right] = \mathrm{Var}\left[\sigma_w^0(\theta_w, d(t))\right] + \mathrm{Var}\left[\sigma'(d(t))\right] \cdot \Delta\theta_d^2 + \frac{1}{4} \cdot \mathrm{Var}\left[\sigma''(d(t))\right] \cdot \Delta\theta_w^4 \tag{25}$$

where the terms $\mathrm{Var}[\sigma_d^0(\theta_d, d(t))]$ and $\mathrm{Var}[\sigma_w^0(\theta_w, d(t))]$ are unknown and set to zero. Hence, the total error is governed solely by the uncertainties in the slope and curvature parameters when interpolating the dry and wet reference to 40°.

By proceeding with the error propagation, the resulting uncertainty in soil moisture can be expressed as follows:

$$\mathrm{Var}\left[m_s(t)\right] = \mathrm{Var}\left[\sigma^0(40,t)\right] \cdot x^2 + \mathrm{Var}\left[\sigma_d^0(40, d(t))\right] \cdot (y-x)^2 + \mathrm{Var}\left[\sigma_w^0(40, d(t))\right] \cdot y^2 \tag{26}$$

with

$$x = \frac{b-a}{\sigma_w^0(40, d(t)) - \sigma_d^0(40, d(t))} \tag{27}$$

$$y = (b-a) \cdot \frac{\sigma^0(40,t) - \sigma_d^0(40, d(t))}{\left(\sigma_w^0(40, d(t)) - \sigma_d^0(40, d(t))\right)^2} \tag{28}$$

It is worth noting that the error model employed is not designed to capture error sources arising under conditions such as frozen soil, snow cover, subsurface scattering, or wetlands. In these environments, the backscatter signal is influenced by factors other than soil moisture, and as such, both noise estimation and soil moisture retrieval may be compromised.

3.4 Advisory flags

Along with the ASCAT SSM datasets, advisory flags are provided to give context on soil conditions, land cover, and scattering behaviour. As previously mentioned, the error model does not account for all potential error sources. These flags complement the error model by helping to identify and filter spatial and temporal situations where soil moisture retrieval may be unreliable.

3.4.1 Wetland fraction flag

As the C-band pulses do not penetrate into water, backscatter characteristics are primarily controlled by the roughness of the water. A calm water surface behaves as a specular reflector, directing almost the entire signal away from the sensor. In contrast, wind-induced waves increase backscatter in both upwind and downwind directions while reducing the signal observed perpendicular to the wind. Consequently, extensive open water within the sensor footprint can significantly interfere with the retrieval of soil moisture. Areas with (temporary) standing water therefore require careful consideration. To address

https://doi.org/10.5194/essd-2025-746
Preprint. Discussion started: 2 February 2026

this, information on the extent of lakes, reservoirs, and large rivers is incorporated by aggregating pixel counts within a defined spatial window, thereby quantifying the maximum water body coverage for each area on a scale from 0 to 100 %.

The wetland fraction flag only indicates the presence of surface water and does not quantify the specific degree of influence a water body may have on the backscatter signal, as this effect can vary depending on factors such as water body size, orientation, or local wind conditions.

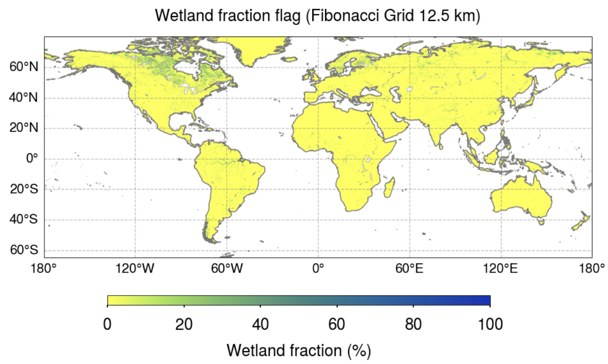

Figure 5. Wetland fraction flag on the Fibonacci Grid 12.5 km.

3.4.2 Topographic complexity flag

Land surfaces characterized by rough terrain and mountainous regions are particularly vulnerable to distortions in backscatter signals arising from varying viewing geometries. Such variability in backscatter adversely affects the accurate retrieval of soil moisture dynamics. To address this limitation, a topographic complexity flag has been introduced. This flag is derived from the Copernicus Digital Elevation Model (COP-DEM) at a spatial resolution of 90 m and provides a quantitative measure of topographic variability. Specifically, it is calculated as the standard deviation of elevation and normalised to a scale from 0 to 100 %. While in these regions observation noise is typically higher, the topographic complexity flag offers users an additional criterion to identify and mask such areas.

3.4.3 Frozen soil probability

When the soil is frozen, microwave backscatter drops significantly due to restricted mobility of soil water molecules, which limits their dielectric response (Hallikainen et al., 1985; Ulaby et al., 1982). In vegetated areas, the interpretation of the backscatter signal becomes more complex because the water content and physical structure of the vegetation further influence the microwave response. Handling backscatter from soil freezing periods is not covered by the soil moisture retrieval algorithm and affected time periods need to be masked based on auxiliary information.

To quantify the likelihood of soil freezing, we derived the frozen soil probability from ERA5 soil temperature (1980–2020). For each grid point and day of year, the probability is defined as the fraction of years with soil temperatures below 0°C.

https://doi.org/10.5194/essd-2025-746
Preprint. Discussion started: 2 February 2026

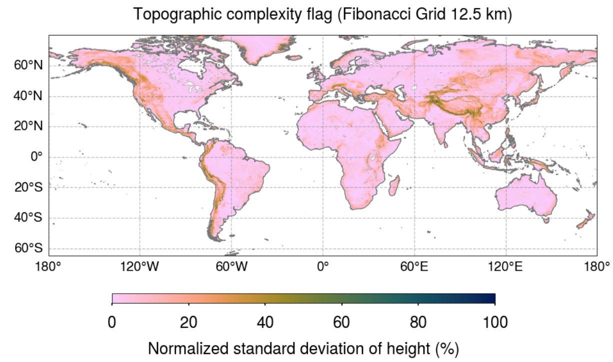

Figure 6. Topographic complexity flag on the Fibonacci Grid 12.5 km.

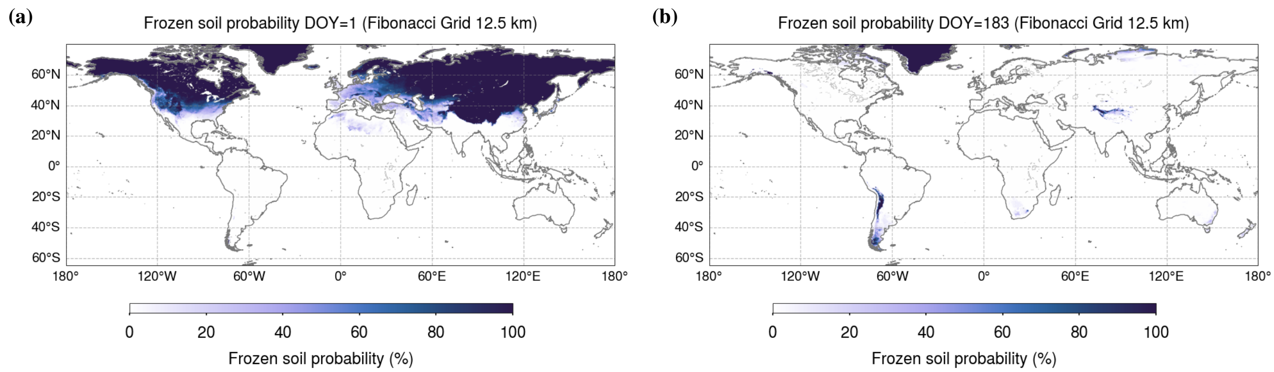

Figure 7. Frozen soil probability flag for (a) day of year (DOY) 1, corresponding to January 1, and (b) DOY 183, corresponding to July 1 on the Fibonacci Grid 12.5 km.

3.4.4 Snow cover probability

The interaction of microwave backscatter with snow is governed by various physical properties of the snow layer, including liquid water content, roughness of the air-snow interface, depth and layering of the snow pack, grain size and shape (Hallikainen et al., 1986; Ulaby et al., 1986). These properties influence the overall backscatter signal through distinct scattering mechanisms (Wismann, 2000). Snow-related scattering effects are not treated in the soil moisture retrieval algorithm and snow covered periods need to be masked based on auxiliary information, e.g. using snow cover information from a land surface model.

Similar to the frozen soil probability, we computed a daily snow probability using ERA5 snow depth data over a 40-year period (1980–2020). For each grid point and day of year, the snow probability is defined as the fraction of years in which snow depth exceeded zero.

https://doi.org/10.5194/essd-2025-746
Preprint. Discussion started: 2 February 2026

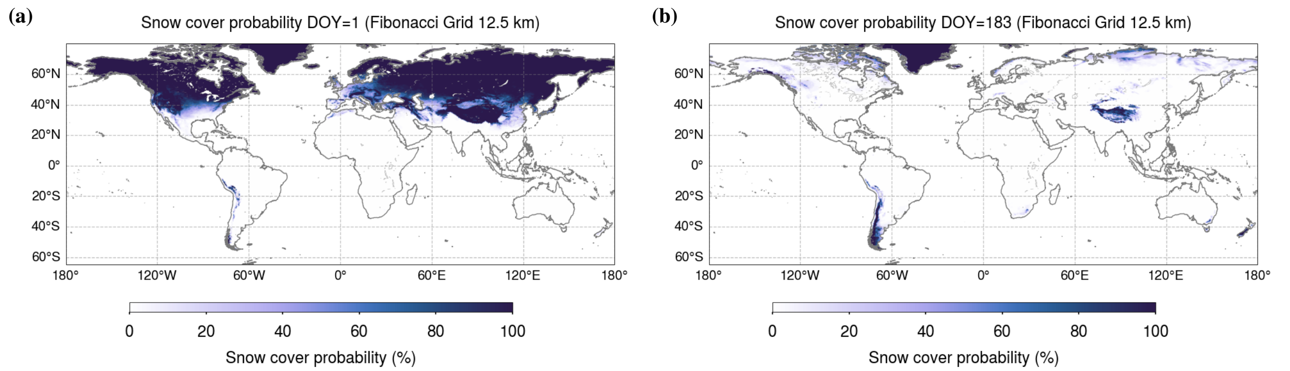

Figure 8. Snow cover probability flag for (a) day of year (DOY) 1, corresponding to January 1, and (b) DOY 183, corresponding to July 1 on the Fibonacci Grid 12.5 km.

3.5 Validation procedure

Quality control of the ASCAT SSM datasets follows standardised validation methodologies for satellite-based Earth observation products (Loew et al., 2017; Land Product Validation Subgroup (Working Group On Calibration And Validation Committee On Earth Observation Satellites), 2020). This process involves quality checking and harmonisation of the reference and ancillary datasets, followed by their spatial and temporal collocation to allow consistent inter-comparison. Finally, relevant quality metrics are calculated and systematically analysed.

For the ASCAT SSM datasets, quality control is performed using soil moisture estimates from Noah GLDAS-2.1 and the ESA CCI Passive Soil Moisture (SM) v09.1 product, as well as in-situ observations provided by the International Soil Moisture Network (ISMN). Ancillary information provided by ERA5 is used to filter out ASCAT SSM observations influenced by frozen soil (skin temperature $< 0°C$) or snow cover (> 0 m). Additionally, internal quality flags from the ASCAT SSM datasets are applied to mask observations affected by subsurface scattering (subsurface scattering probability $> 5\,\%$).

In case of the global analysis against ESA CCI Passive SM and GLDAS-2.1, the fixed Earth grid of the ASCAT SSM datasets served as the spatial reference, with all other datasets collocated using a nearest neighbour search. Temporal collocation is based on the measurement times of the ASCAT SSM datasets. For each ASCAT SSM observation, the temporally closest reference measurement within an 12-hour window is selected. The Pearson correlation coefficient (R) and Signal-to-Noise Ratio (SNR) are used as the two main quality metrics. While Pearson R quantifies the strength and direction of a linear relationship between two datasets, SNR is derived from triple collocation analysis (TCA) (Stoffelen, 1998), which estimates error variance by comparing three independent datasets. By relating the error variance to the signal variance, the SNR quantifies the relative strength between the signal and noise. Expressed in decibel (dB), the SNR provides an intuitive interpretation (Gruber et al., 2016).

The Quality Assurance Service for Satellite Soil Moisture Data (QA4SM) was used for the validation against ISMN observations (AWST, TU Wien, CESBIO, 2025). ASCAT SSM time series were extracted from the grid points nearest to the ISMN

https://doi.org/10.5194/essd-2025-746
Preprint. Discussion started: 2 February 2026

station coordinates and uploaded to the QA4SM portal. ISMN networks with sensors overlapping in time with the ASCAT SSM datasets and operating within the 0–10 cm depth range were selected. A 12-hour matching window was applied to identify the nearest observation in time. The Pearson correlation coefficient (R) served as the primary performance metric.

4 Results and discussion

4.1 ASCAT Surface Soil Moisture datasets

As described in Sect. 3, the ASCAT SSM datasets are generated with two spatial sampling distances: 6.25 km and 12.5 km. These datasets are distributed as part of the EUMETSAT Satellite Application Facility on Support to Operational Hydrology and Water Management (H SAF) product suite. H SAF aims to provide remote sensing products of hydrological parameters including instantaneous rain rate and accumulated rainfall, surface soil moisture and root zone soil moisture, as well as snow cover and snow water equivalent.

H SAF products are categorized based on their timeliness into three categories: near real-time (NRT), offline, and data records (DR). NRT products offer the lowest latency, providing rapid access. Offline products are available on a daily, weekly, or monthly basis, accommodating a range of application. DR products represent fixed datasets with well defined start and end dates, suitable for climate analysis. If a DR product spans more than 15 years, it is referred to as a climate data record (CDR). Furthermore, if an offline product uses the same processing chain and input data as a (C)DR and serves to extend it beyond its original time span, it is referred to as an interim data record (IDR) or interim climate data record (ICDR).

The ASCAT SSM datasets are provided as NRT, CDR, and ICDR products as outlined in Table 3. All datasets are available through the H SAF online archive, while NRT products are additionally distributed via EUMETCast, a satellite-based broadcast system operated by EUMETSAT. The primary data format is netCDF, with BUFR (Binary Universal Form for the Representation of meteorological data) being also available for selected products.

Table 3. ASCAT Soil Surface Moisture (SSM) datasets provided by EUMETSAT H SAF. All datasets are classified as Level 2 products, except for the Disaggregated (DIS) ASCAT SSM NRT v2 0.5 km product, which is Level 3 product since it represents a downscaled version of the ASCAT SSM NRT 6.25 km product.

Product ID	Acronym	Category	Spatial sampling	Temporal coverage	Data format
H121	ASCAT SSM CDR v8 12.5 km	CDR	12.5 km	2007-01-01–2024-12-31	netCDF, BUFR
H139	ASCAT SSM CDR v8 EXT 12.5 km	ICDR	12.5 km	2025-01-01–ongoing	netCDF
H29	ASCAT SSM NRT v2 12.5 km	NRT	12.5 km	2025-07–ongoing	netCDF, BUFR
H129	ASCAT SSM CDR v1 6.25 km	CDR	6.25 km	2007-01-01–2024-12-31	netCDF
H130	ASCAT SSM CDR v1 EXT 6.25 km	ICDR	6.25 km	2025-01-01–ongoing	netCDF
H122	ASCAT SSM NRT 6.25 km	NRT	6.25 km	2025-07–ongoing	netCDF
H28	DIS ASCAT SSM NRT v2 0.5 km	NRT	0.5 km	2025-07–ongoing	netCDF

https://doi.org/10.5194/essd-2025-746
Preprint. Discussion started: 2 February 2026

4.1.1 Data characteristics

The ASCAT SSM datasets are supplied in swath orbit geometry, with observations resampled onto a fixed Earth grid. For this purpose, the Fibonacci grid has been selected (see Sect. 3.1.2), ensuring a homogeneous sampling of the Earth's surface. The ASCAT SSM CDR and ICDR consists of swath data covering 60-minute interval, whereas the ASCAT SSM NRT datasets are distributed in 3-minute product dissemination units (PDUs). Figure 9 shows an example for both swath intervals. All ASCAT SSM datasets (CDR, ICDR, NRT) delivered in netCDF contain an identical set of variables, as listed in Table 4.

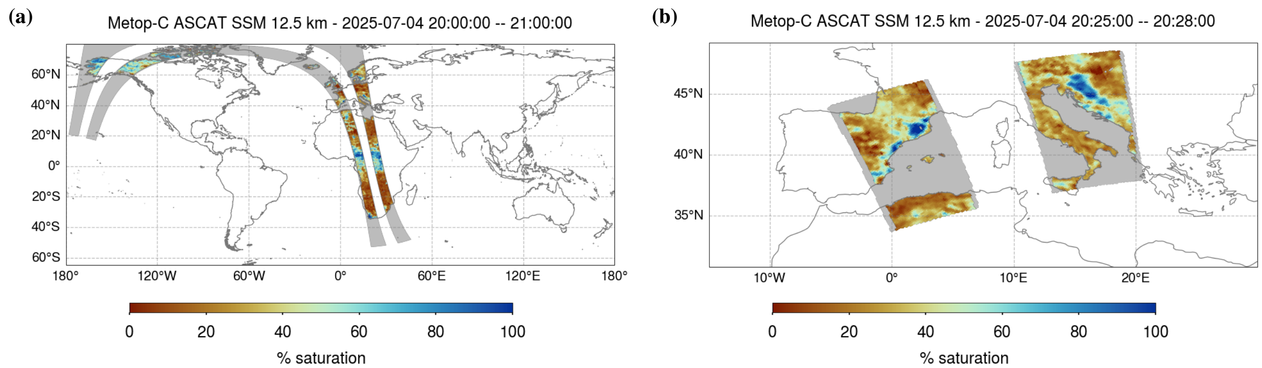

Figure 9. Example ASCAT SSM swath for a 60-minute (a) and 3-minute (b) interval.

Surface soil moisture (SSM) and its associated noise are the primary variables provided in the ASCAT SSM datasets. Both, SSM and SSM noise are expressed in degree of saturation representing the topmost soil layer (< 5 cm). The SSM sensitivity is quantified in decibels (dB) and defined as the difference between the wet and dry backscatter references for a given day (see Sect. 3.3.6). It also serves as an indicator of retrieval uncertainty with values below 1 dB typically pointing to densely vegetated areas with a low backscatter signal variation. Backscatter at 40° incidence angle, as well as the first and second derivatives (slope and curvature) of the incidence angle dependency of backscatter, are included to provide additional information. Furthermore, flags inform about surface conditions or processing details (see Sect. 3.4). Time and geo-location parameters are expressed as fractions of days since the reference date 1970-01-01 00:00:00 UTC and latitude/longitude coordinates (EPSG:4326) along with a unique location identifier. Moreover, satellite orbit direction (ascending/descending) and swath identification (left/right) are included.

Since ASCAT SSM datasets are provided on a fixed Earth grid, time series can be readily generated by stacking individual swath segments. As each observation is associated with a unique timestamp and the number of observations varies by location, not all locations have the same number of measurements. Therefore, storing the time series data as an indexed ragged array is more storage-efficient than using an incomplete multidimensional array representation, which requires padding unused elements with missing values. If all locations share the same number of observations, the latter is referred to as an orthogonal multidimensional array representation. Space-time cubes derived from gridded raster data are a classical example. However, it is not well suited for observations from polar-orbiting LEO satellites, where coverage varies due to the swath geometry and

https://doi.org/10.5194/essd-2025-746
Preprint. Discussion started: 2 February 2026

Table 4. Description of ASCAT SSM dataset variables and associated metadata.

Variable	Unit	Description
surface_soil_moisture	%	Surface soil moisture (< 5 cm)
surface_soil_moisture_noise	%	Uncertainty of surface soil moisture
surface_soil_moisture_sensitivity	dB	Sensitivity of backscatter to changes in soil moisture
backscatter40	dB	Backscatter at 40° incidence angle
slope40	$\mathrm{dB\,deg^{-1}}$	First derivative at 40° incidence angle, i.e. slope
curvature40	$\mathrm{dB\,deg^{-2}}$	Second derivative at 40° incidence angle, i.e. curvature
frozen_soil_probability	%	Frozen soil probability (derived using ERA5 soil temperature)
snow_cover_probability	%	Snow cover probability (derived using ERA5 snow cover)
wetland_fraction	%	Wetland fraction (derived using GLWD)
topographic_complexity	%	Topographic complexity (derived using Copernicus DEM)
subsurface_scattering_probability	%	Probability of subsurface scattering
surface_flag	flag table	Encodes land/water, snow, and frozen soil conditions
processing_flag	flag table	Encodes why surface soil moisture is unavailable
correction_flag	flag table	Encodes corrections applied during data processing
location_id	-	Unique location identifier (starting at 0)
latitude	degrees north	Latitude coordinate (EPSG:4326)
longitude	degrees east	Longitude coordinate (EPSG:4326)
as_des_pass	code table	Orbit direction (0=ascending, 1=descending)
swath_indicator	code table	Swath indicator (0=left, 1=right)

orbital dynamics. Figure 10 illustrates the spatial coverage of ASCAT for a single and two Metop satellites over a 24-hour period.

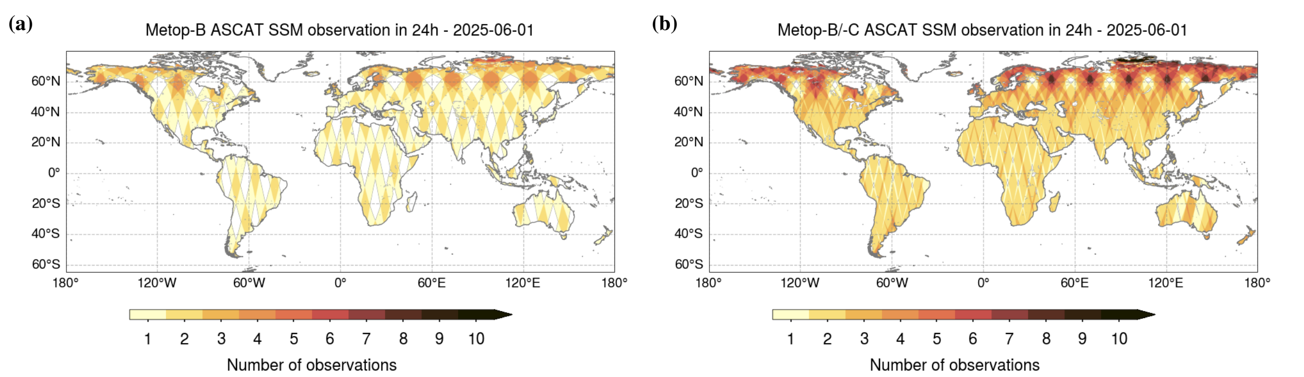

Figure 10. ASCAT observations recorded within a 24-hour period over land: (a) Metop-B only, (b) combined Metop-B and Metop-C data.

https://doi.org/10.5194/essd-2025-746
Preprint. Discussion started: 2 February 2026

The ascat Python package provides utility functions for converting a collection of swath files into time series format (Hahn et al., 2025). During this process, a satellite identifier variable is added to each observation to preserve information about the source platform. Figure 11 shows an example SSM and soil water index (SWI) time series over central Italy. SWI is computed using an exponential filter of SSM, which mimics water infiltration into deeper soil layers (Wagner et al., 1999b; Albergel et al., 2008). The characteristic time length (T) represents the "memory" or depth response. SSM is highly sensitive to atmospheric forcing, including precipitation, evaporation, wind, and solar radiation, and therefore exhibits pronounced short-term variability. In contrast, SWI attenuates these rapid fluctuations and is commonly employed as a proxy for soil moisture in deeper layers (Paulik et al., 2014). SSM and SWI anomalies, calculated as deviations from their long-term climatological means, serve as valuable indicator of hydrological extremes or shifts in land surface conditions.

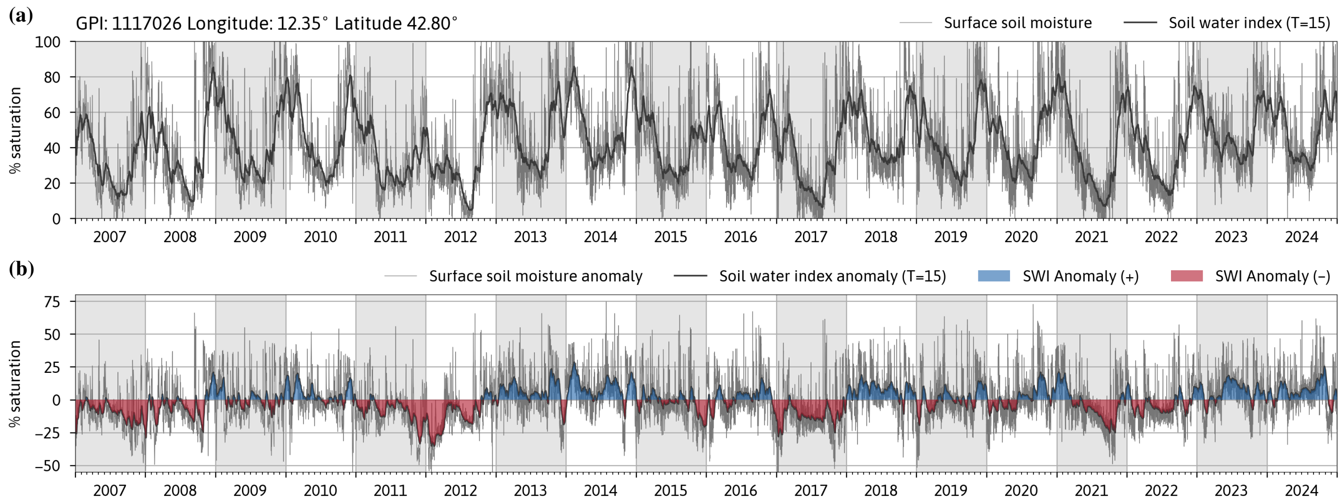

Figure 11. Example ASCAT SSM time series for a grid point in central Italy. The top time series (a) shows soil water index (SWI) derived from the original SSM, while the bottom time series (b) illustrates the anomalies of both SSM and SWI.

4.2 Comparison against ESA CCI Passive SM and Noah GLDAS-2.1

Quality assessment was performed as outlined in Sect. 3.5. The main performance metrics are the Pearson correlation coefficient (R) and Signal-to-Noise Ratio (SNR). The validation covered the time period from 2007-01-01 until 2023-12-31 in case of both reference datasets.

4.2.1 Pearson correlation

Figures 12 and 13 present global maps of the Pearson correlation coefficient (R) along with the corresponding number of observation pairs. In case of Pearson R between ASCAT SSM 6.25 km and ESA CCI Passive SM, 17.9 % of grid points are above 0.75 and 57.8 % are higher than 0.5 (see Figure 12a). Similar results can be seen for ASCAT SSM 12.5 km as well, with 19.6 % grid points above 0.75 and 59.2 % higher than 0.5 (see Figure 12c). In general, lower performance is observed in regions

https://doi.org/10.5194/essd-2025-746
Preprint. Discussion started: 2 February 2026

with limited soil moisture variability, such as deserts, as well as at higher latitudes where the soil remains frozen or covered by snow for extended periods and validation is consequently restricted to summer months. In contrast, the best performance is found in areas with strong seasonal variability, including monsoonal, savanna, Mediterranean, and tropical wet-and-dry climate zones.

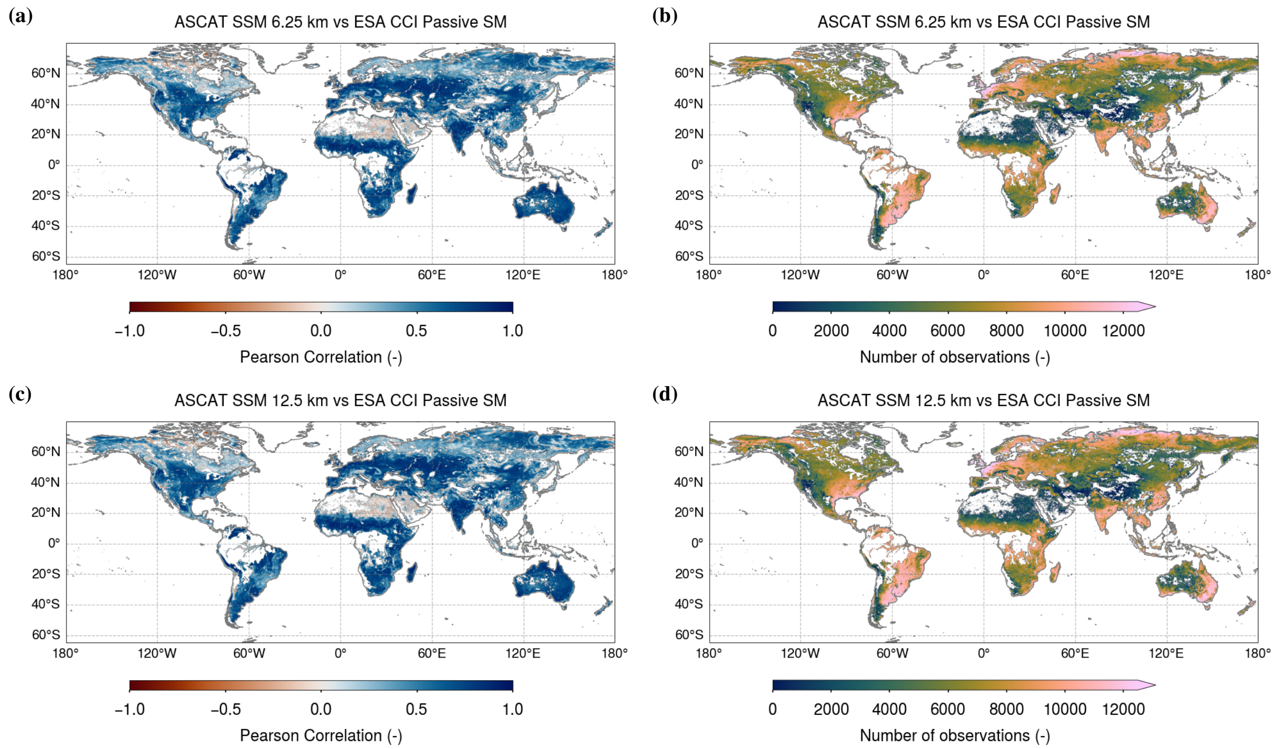

Figure 12. Global maps of the Pearson correlation coefficient (a) and the number of observation pairs (b) between ASCAT SSM at 6.25 km and ESA CCI Passive SM are shown in the top half, while corresponding maps for ASCAT SSM at 12.5 km (c, d) are presented in the bottom half.

A similar pattern can be seen in the results of Pearson R between ASCAT SSM 6.25 km and Noah GLDAS-2.1 SM with 13.1 % grid points above 0.75 and 45.9 % higher than 0.5 (see Figure 13a) and 14.5 % grid points above 0.75 and 47.7 % higher than 0.5 looking at ASCAT SSM 12.5 km (see Figure 13c). In comparison to ESA CCI Passive SM, fewer regions have been masked, allowing densely vegetated areas such as the Amazon, Congo, and Indonesian rainforests to be included in the analysis. This reveals the lower performance of the ASCAT SSM datasets in these regions, where dense canopy cover reduces the sensitivity of backscatter signals to soil moisture changes. Notably, these areas could be excluded by applying the soil moisture sensitivity information (< 1 dB) available in the ASCAT SSM datasets (see Table 4).

Figures 12a, c and 13a, c show no significant performance differences of Pearson R between ASCAT SSM 6.25 km and 12.5 km. However, there are consistent, albeit small, differences indicating slightly higher Pearson R values for ASCAT SSM 12.5 km. When comparing the Pearson R values (ASCAT SSM 6.25 km minus ASCAT SSM 12.5 km using nearest neighbour

https://doi.org/10.5194/essd-2025-746
Preprint. Discussion started: 2 February 2026

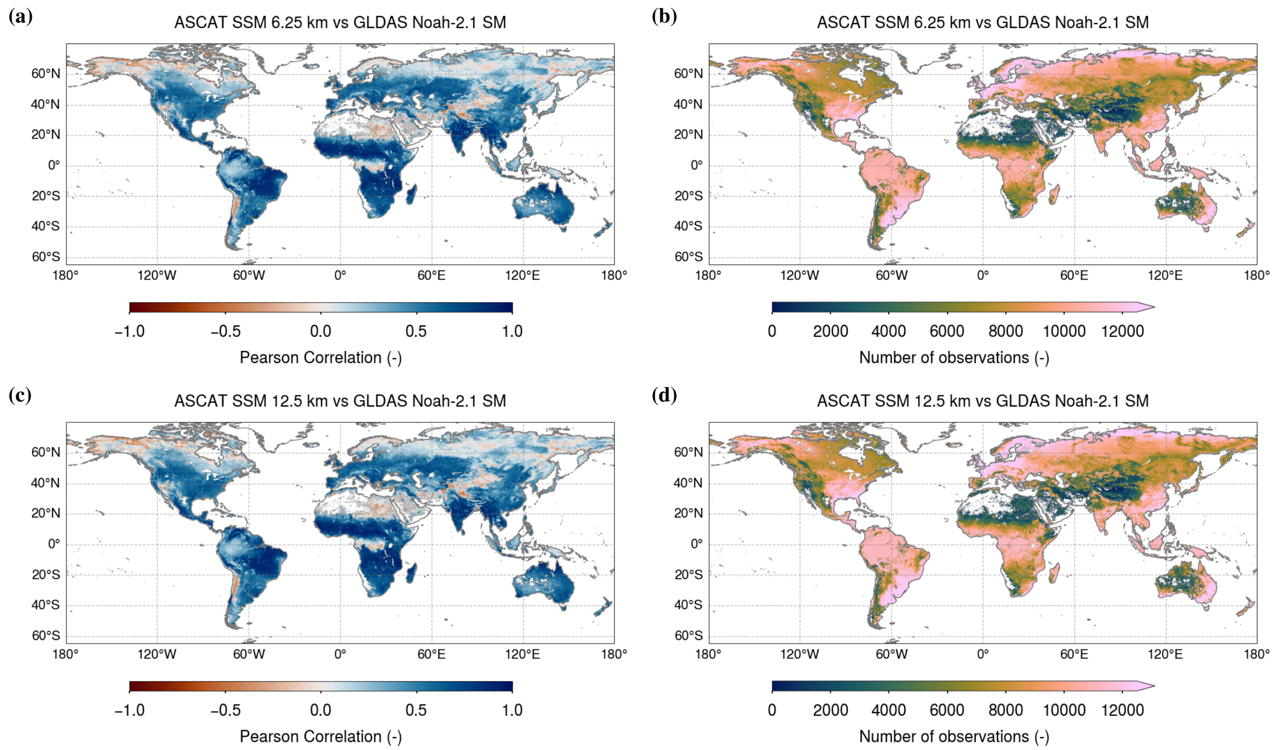

Figure 13. Global maps of the Pearson correlation coefficient (a) and the number of observation pairs (b) between ASCAT SSM at 6.25 km and Noah GLDAS-2.1 are shown in the top half, while corresponding maps for ASCAT SSM at 12.5 km (c, d) are presented in the bottom half.

grid points), the inter-quartile range (IQR) varies between 0.0 and -0.2 for both ESA CCI Passive SM and Noah GLDAS-2.1. This observed behaviour can be expected since ASCAT SSM 6.25 km is anticipated to exhibit more spatio-temporal fluctuations and noise compared to ASCAT SSM 12.5 km. In fact, the new ASCAT SSM 6.25 km dataset demonstrated a robust performance, even in the absence of globally comparable reference datasets for validation. While direct comparisons against the reference data used for the 12.5 km product is not fully appropriate due to the scale mismatch, the ASCAT SSM 6.25 km product shows a strong agreement. This performance underscores its potential value for applications requiring SSM at higher spatial resolution.

4.2.2 Signal-to-Noise Ratio (SNR)

Figure 14a and c illustrate the Signal-to-Noise Ratio (SNR) computed between the ASCAT SSM datasets, ESA CCI Passive SM and Noah GLDAS-2.1 SM. In case of ASCAT SSM 6.25 km, more than 35.6 % grid points show a SNR higher than 3 dB, while 56.0 % are above 0 dB. Comparing the results against ASCAT SSM 12.5 km shows minor improvements with 38.6 % (SNR > 3 dB) and 58.1 % (SNR > 0 dB), respectively. In contrast to the Pearson correlation coefficient (R), which may

https://doi.org/10.5194/essd-2025-746
Preprint. Discussion started: 2 February 2026

remain high despite substantial noise, the SNR derived from triple collocation analysis (TCA) is a more fundamental metric. It explicitly quantifies the relative contribution of signal and noise, thereby providing a more critical assessment of data quality. This is evident in many regions with low soil moisture variability, where the SNR becomes negative indicating a higher noise variance with respect to the signal component (e.g. desert areas of Africa, the Arabian Peninsula, central Australia, and North America). Similarly, in high-latitude regions where the Pearson R is weakly positive, the SNR becomes negative. As previously mentioned, validation of the full seasonal cycle is not always feasible due to the presence of frozen soils or persistent snow cover. This limitation poses a challenge for a comprehensive validation and interpretation. Therefore, a negative SNR should not be interpreted as evidence that the ASCAT SSM datasets are unusable in these regions. Instead, it signals challenges arising from environmental factors. Users are always advised to take local conditions into account when interpreting remote sensing soil moisture datasets.

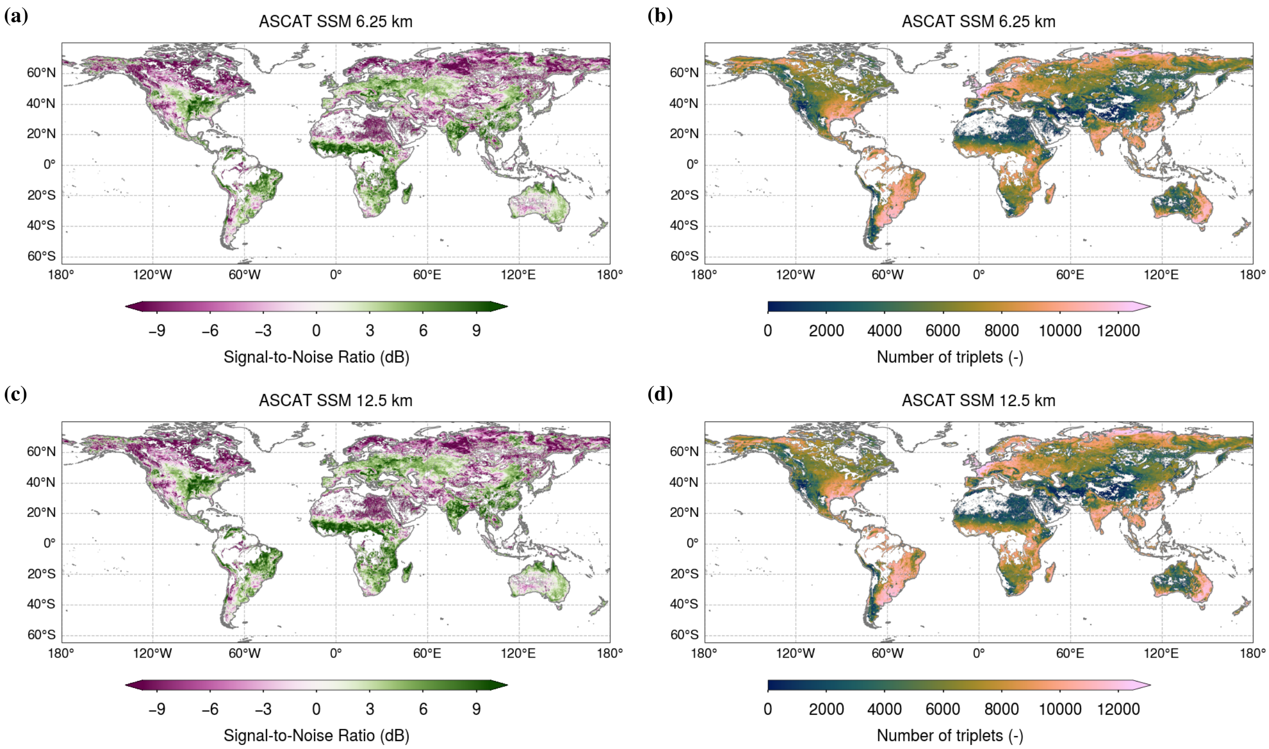

Figure 14. Global maps of Signal-to-Noise Ratio (SNR) (a) and the number of triplets (b) between ASCAT SSM 6.25 km, Noah GLDAS-2.1 and ESA CCI Passive SM are shown in the top half, while corresponding maps for ASCAT SSM 12.5 km (c, d) are presented in the bottom half.

Based on the SNR performance evaluation, there is no significant difference between ASCAT SSM 6.25 km and 12.5 km datasets (see Figures 14a, c). However, a point-wise comparison of SNR (ASCAT SSM 6.25 km minus ASCAT SSM 12.5 km using nearest neighbour grid points) reveals that the inter-quartile range (IQR) varies between 0.3 and -0.6 dB. As discussed for Pearson R, a slightly better performance can be anticipated due to higher spatio-temporal frequencies in ASCAT SSM

https://doi.org/10.5194/essd-2025-746
Preprint. Discussion started: 2 February 2026

6.25 km compared to ASCAT SSM 12.5 km. Overall, these small SNR differences confirm that the higher-resolution ASCAT SSM 6.25 km dataset does not introduce substantial noise.

4.3 Comparison against ISMN

A total of 44 in-situ networks from the International Soil Moisture Network (ISMN) that temporally overlap with the ASCAT SSM datasets were used for validation (Table A1). For each network, sensors measuring within the 0–10 cm depth range were primarily selected. Figure 15 shows boxplots of the Pearson correlation coefficient (R) for each network, with the number of sensors next to the network name.

The inter-quartile range (IQR) of the boxplots lies between the interval 0.25 and 0.85, with over two-thirds of the networks indicating a 25th percentile (lower bound of the IQR) above 0.5. The highest performance of the ASCAT SSM datasets is observed for the networks CTP_SMTMN, NAQU, REMEDHUS, SASMAS, and THAMO. In contrast, 24 sensors from three networks (SCAN, SNOTEL, and USCRN) yield negative Pearson R values. All of these sensors are located in the United States (California, Nevada, and Utah), with more than 90 % situated at elevations above 2000 m. The combination of arid climate, limited signal variability, complex topography and the presence of subsurface scattering effects likely explains the reduced performance in these regions.

While the overall distributions of Pearson R values remain similar for both ASCAT SSM datasets, their median values show minor network-specific variations. Specifically, the ASCAT SSM 6.25 km dataset shows slightly higher medians for DAHRA, RISMA, and SNOTEL, whereas the 12.5 km dataset performs marginally better for HOAL, SCAN, USCRN, and WSMN. Neither resolution consistently outperforms the other and the differences observed are small in magnitude.

A comparison of our Pearson R evaluation between the ASCAT SSM datasets and the ISMN networks with previous studies based on earlier versions of ASCAT SSM datasets indicates generally consistent performance (e.g., Fascetti et al. (2016); Al-Yaari et al. (2019); Beck et al. (2021); Mazzariello et al. (2023)). However, a direct comparison of results remains challenging due to differences in the input datasets, applied pre-processing steps and overall validation setup.

5 Conclusions

This article introduces the first ASCAT surface soil moisture (SSM) dataset generated at a nominal sampling of 6.25 km, alongside the standard 12.5 km sampling commonly used in previous ASCAT SSM dataset versions (H SAF, 2017, 2020, 2021). The ASCAT SSM datasets are available as near real-time (NRT), climate data record (CDR), and interim climate data record (ICDR) products and distributed through the H SAF online archive via FTP. The ICDR serves as an extension of the CDR, generated using the same processing chain and input data, while the NRT product priorities timeliness over long-term consistency. ASCAT NRT products are additionally distributed via EUMETCast, a satellite-based broadcast system operated by EUMETSAT.

Both ASCAT SSM datasets presented in this article are generated from ASCAT Level 1B SZF backscatter data using the same semi-empirical change detection algorithm. They differ only in the spatial resampling radius. During the resampling

https://doi.org/10.5194/essd-2025-746
Preprint. Discussion started: 2 February 2026

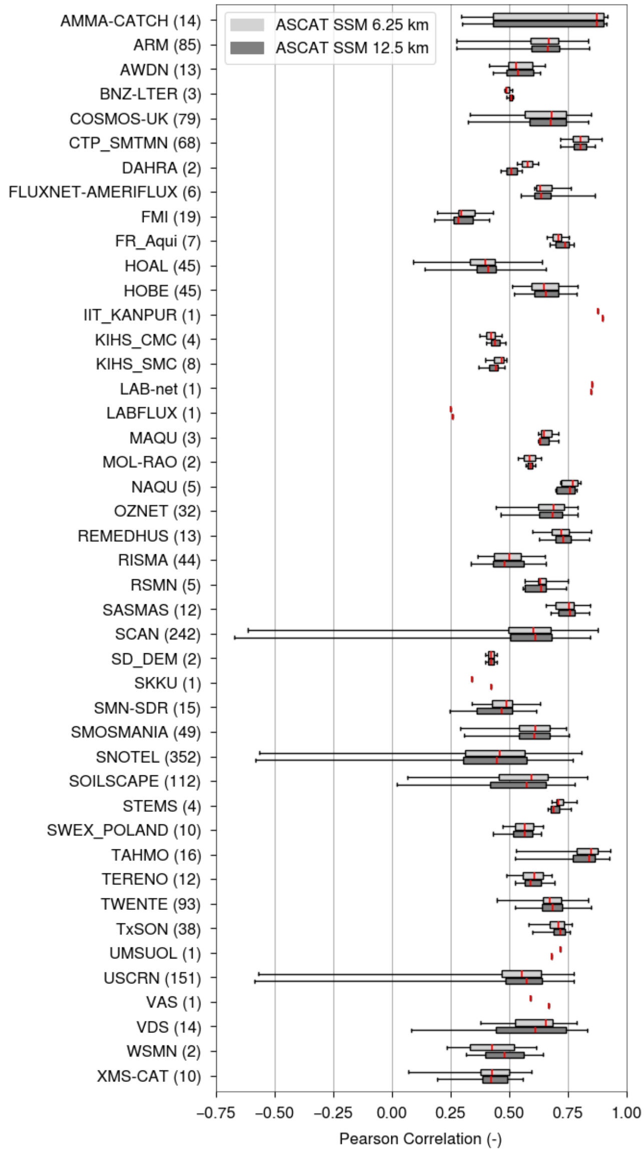

Figure 15. Pearson correlation coefficient (R) computed between ASCAT SSM (6.25 km and 12.5 km) and 44 ISMN in-situ networks. The boxplots depict the distribution of Pearson R for each network, with the number of sensors next to the network name. Whiskers extend to the 2nd and 98th percentiles of the Pearson R distribution per network.

process, backscatter echos over surfaces not sensitive to soil moisture changes (e.g., open water, urban areas) are masked. This masking, combined with the smaller resampling radius of the ASCAT SSM 6.25 km dataset (14 km vs. 24 km), increases the likelihood of reduced or insufficient echo counts, potentially leading to higher noise or, in extreme cases, discontinuities in data coverage. At the same time, the finer spatial resolution of the 6.25 km dataset introduces greater spatio-temporal signal

https://doi.org/10.5194/essd-2025-746
Preprint. Discussion started: 2 February 2026

Open Access Earth System Science Data Discussions

variability. Despite all these effects, global validation against Noah GLDAS-2.1 and ESA CCI Passive v09.1, along with comparisons to 44 ISMN in-situ networks, demonstrates that the ASCAT SSM 6.25 km dataset achieves a Pearson R and SNR performance equivalent to that of the standard 12.5 km product. Minor, yet consistent, differences were observed in the global validation, which are small and expected given that the reference datasets do not share the same spatial resolution as the ASCAT SSM 6.25 km product.

Overall, the validation results indicate best performance of ASCAT SSM in regions with strong seasonal variability, including monsoonal, savanna, Mediterranean, and tropical wet-and-dry zones. In contrast, a lower performance can be found in areas characterised by limited soil moisture variability (e.g., deserts), dense vegetation, pronounced topographic complexity, wetlands, or higher latitudes (> 60° N). Degradation in these regions is driven by distinct mechanisms. Limited soil moisture variability in arid regions reduces the signal dynamic range, undermining the statistical robustness. Dense vegetation attenuates the microwave signal through canopy absorption and volume scattering, effectively masking soil surface conditions. Pronounced topographic complexity introduces heterogeneous scattering patterns that overlay with soil moisture contributions. Large wetlands with standing water either generate strong specular reflection or further complicate the backscatter signal response by emergent vegetation that creates more complex scattering effects. Finally, higher latitudes experience longer periods of frozen soil and snow cover, which disrupts the physical relationship between microwave backscatter and liquid soil moisture, making the signal insensitive or misleading. Thus, the change detection algorithm used to derived the ASCAT SSM datasets performs optimally under conditions of: (i) low to moderate vegetation density, (ii) unfrozen and snow-free terrain, (iii) negligible subsurface scattering, (iv) low to moderate topographic complexity, (v) absence of wetlands, and (vi) absence of radio frequency interference (RFI).

The Metop-Second Generation (Metop-SG) B-series satellites (Metop-SG B1 scheduled for launch in 2026), will carry the next-generation scatterometer (SCA). Sharing an instrument design similar to ASCAT, SCA will enable a seamless continuity of soil moisture datasets. Furthermore, SCA features key enhancements over ASCAT including an improved radiometric resolution and an additional VH- and HH-channel on both left and right Mid beams. These upgrades create new opportunities to refine the soil moisture retrieval algorithm. Finally, and most importantly, operational continuity from ASCAT to SCA, combined with cross-calibration against the ERS-1 and ERS-2 missions, will establish a unique, multi-decade dataset essential for global climate change research.

6 Data availability

The ASCAT Surface Soil Moisture (SSM) datasets are available in netCDF swath file format https://doi.org/10.15770/EUM_SAF_H_0011 and https://doi.org/10.15770/EUM_SAF_H_0012 (H SAF, 2025a, c). The ASCAT SSM climate data records (CDR) are provided globally (180° W 65° S - 180° E 80° N) and cover the time period 2007-01-01 until 2024-12-31. Soil moisture is expressed in degree of saturation (0% dry soil, 100% saturated soil) representing the topmost soil layer (< 5 cm). Advisory flags are included to give context on soil state, land cover, and scattering behaviour. Users are encouraged to apply these flags to

https://doi.org/10.5194/essd-2025-746
Preprint. Discussion started: 2 February 2026

exclude time periods or locations influenced by frozen soil or snow cover prior to data usage. When available, external datasets on soil temperature and snow cover should also be used to refine this filtering.

660 **Appendix A: In-situ**

Table A1: In situ soil moisture networks used for validation.

Network	Country	Period	Reference
AMMA-CATCH	Benin, Niger, Mali	2006-01-01 to 2018-12-31	Pellarin et al. (2009); Mougin et al. (2009); Cappelaere et al. (2009); de Rosnay et al. (2009); Lebel et al. (2009); Galle et al. (2015)
ARM	USA	1993-06-29 to 2025-09-07	Cook (2016a, b)
AWDN	USA	1997-12-31 to 2010-12-30	-
BNZ-LTER	USA	1988-06-01 to 2013-01-01	-
COSMOS-UK	UK	2013-10-02 to 2023-01-01	Cooper et al. (2021)
CTP_SMTMN	China	2010-08-01 to 2016-09-19	Yang et al. (2013)
DAHRA	Senegal	2002-07-04 to 2016-01-01	Tagesson et al. (2014)
FLUXNET-AMERIFLUX	USA	2000-01-01 to 2020-07-21	-
FMI	Finland	2007-01-25 to 2025-09-06	Ikonen et al. (2016)
FR_Aqui	France	2012-01-01 to 2025-01-01	Al-Yaari et al. (2018); Wigneron et al. (2018)
HOAL	Austria	2013-07-11 to 2021-12-31	Blöschl et al. (2016); Vreugdenhil et al. (2013)
HOBE	Denmark	2009-09-08 to 2019-03-13	Bircher et al. (2012); Jensen and Refsgaard (2018)
IIT_KANPUR	India	2011-06-16 to 2012-11-22	-
IPE	Spain	2008-04-03 to 2020-03-25	Alday et al. (2020)
KIHS_CMC	South Korea	2008-06-20 to 2019-12-10	-
KIHS_SMC	South Korea	2007-06-06 to 2019-12-05	-
LAB-net	Chile	2014-07-18 to 2020-07-14	Mattar et al. (2014, 2016)
LABFLUX	Italy	2015-01-27 to 2025-04-14	-
MAQU	China	2008-05-13 to 2019-06-01	Su et al. (2011); Dente et al. (2012)

https://doi.org/10.5194/essd-2025-746
Preprint. Discussion started: 2 February 2026

Network	Country	Period	Reference
MOL-RAO	Germany	2003-01-01 to 2020-06-30	Beyrich and Adam (2007)
NAQU	China	2010-06-15 to 2019-09-12	Su et al. (2011); Dente et al. (2012)
OZNET	Australia	2001-09-12 to 2021-09-01	Young et al. (2008); Smith et al. (2012)
REMEDHUS	Spain	2005-03-15 to 2025-01-01	González-Zamora et al. (2019)
RISMA	Canada	2013-04-24 to 2020-03-25	Ojo et al. (2015)
RSMN	Romania	2014-04-09 to 2025-08-15	-
SASMAN	Australia	2005-12-31 to 2007-12-31	Rüdiger et al. (2007)
SCAN	USA	1996-08-15 to 2025-09-07	Schaefer et al. (2007)
SD_DEM	Sweden	2002-02-08 to 2020-11-12	Ardö (2013)
SKKU	South Korea	2014-05-08 to 2017-11-29	Nguyen et al. (2017)
SMN-SDR	China	2018-07-25 to 2019-12-31	Zhao et al. (2020)
SMOSMANIA	France	2007-01-01 to 2025-01-01	Calvet et al. (2007); Albergel et al. (2008); Calvet et al. (2016)
SNOTEl	USA	1996-09-10 to 2025-09-07	Leavesley et al. (2008)
SOILSCAPE	USA	2011-08-03 to 2025-09-08	Shuman et al. (2010); Moghaddam et al. (2010, 2016)
STEMS	Italy	2015-12-04 to 2025-01-15	Capello et al. (2019); Darouich et al. (2022)
SWEX_POLAND	Poland	2000-01-01 to 2013-05-06	Marczewski et al. (2010)
TAHMO	Côte d'Ivoire, Nigeria, Ghana, Uganda, Rwanda, Kenya	2015-06-17 to 2022-07-07	
TERENO	Germany	2009-12-31 to 2025-07-07	Zacharias et al. (2011); Bogena et al. (2012); Bogena (2016); Bogena et al. (2018)
TWENTE	Netherlands	2008-11-12 to 2020-12-31	van der Velde et al. (2023)
TxSON	USA	2014-10-01 to 2022-11-08	Caldwell et al. (2019)
UMSUOL	Italy	2009-06-12 to 2017-05-15	-
USCRN	USA	2000-11-15 to 2025-09-08	Bell et al. (2013)
VAS	Spain	2010-01-01 to 2012-01-01	-
VDS	Myanmar	2017-06-01 to 2021-02-13	-
WSMN	UK	2011-09-02 to 2016-02-29	Petropoulos and McCalmont (2017)
XMS-CAT	Spain	2016-08-01 to 2025-09-08	-

https://doi.org/10.5194/essd-2025-746
Preprint. Discussion started: 2 February 2026

Author contributions. Sebastian Hahn: Writing, Software Development, Processing, Validation, Visualization. Thomas Melzer: Writing - review & editing, Error characterisation, Backscatter-incidence angle characterisation. Wolfgang Wagner: Writing – review & editing, Original algorithm development, Supervision.

Competing interests. The contact author has declared that none of the authors has any competing interests.

Acknowledgements. The generation of ASCAT SSM datasets was carried out in the framework of the forth SAF Continuous Development and Operations Phase (CDOP 4) of the EUMETSAT Satellite Application Facility on Support to Operational Hydrology and Water Management (H SAF). We thank EUMETSAT and all H SAF consortium members for their continuous support.

https://doi.org/10.5194/essd-2025-746
Preprint. Discussion started: 2 February 2026

References

Aires, F., Weston, P., Rosnay, P., and Fairbairn, D.: Statistical approaches to assimilate ASCAT soil moisture information-I. Methodologies and first assessment, 147, 1823–1852, https://doi.org/10.1002/qj.3997, 2021.

Al-Yaari, A., Dayau, S., Chipeaux, C., Aluome, C., Kruszewski, A., Loustau, D., and Wigneron, J.-P.: The AQUI Soil Moisture Network for Satellite Microwave Remote Sensing Validation in South-Western France, Remote Sensing, 10, 1839, https://doi.org/10.3390/rs10111839, 2018.

Al-Yaari, A., Wigneron, J.-P., Dorigo, W., Colliander, A., Pellarin, T., Hahn, S., Mialon, A., Richaume, P., Fernandez-Moran, R., Fan, L., Kerr, Y., and Lannoy, G. D.: Assessment and inter-comparison of recently developed/reprocessed microwave satellite soil moisture products using ISMN ground-based measurements, Remote Sensing of Environment, 224, 289–303, https://doi.org/10.1016/j.rse.2019.02.008, 2019.

Albergel, C., Rüdiger, C., Pellarin, T., Calvet, J.-C., Fritz, N., Froissard, F., Suquia, D., Petitpa, A., Piguet, B., and Martin, E.: From Near-Surface to Root-Zone Soil Moisture Using an Exponential Filter: An Assessment of the Method Based on in-Situ Observations and Model Simulations, Hydrology and Earth System Sciences, 12, 1323–1337, https://doi.org/10.5194/hess-12-1323-2008, 2008.

Alday, J. G., Camarero, J. J., Revilla, J., and Resco de Dios, V.: Similar diurnal, seasonal and annual rhythms in radial root expansion across two coexisting Mediterranean oak species, Tree Physiology, 40, 956–968, https://doi.org/10.1093/treephys/tpaa041, 2020.

Álvaro González: Measurement of Areas on a Sphere Using Fibonacci and Latitude–Longitude Lattices, Mathematical Geosciences, 42, 49–64, https://doi.org/10.1007/s11004-009-9257-x, 2009.

Anderson, C., Figa, J., Bonekamp, H., Wilson, J. J. W., Verspeek, J., Stoffelen, A., and Portabella, M.: Validation of Backscatter Measurements from the Advanced Scatterometer on MetOp-A, Journal of Atmospheric and Oceanic Technology, 29, 77–88, https://doi.org/10.1175/JTECH-D-11-00020.1, 2012.

Ardö, J.: A 10-Year Dataset of Basic Meteorology and Soil Properties in Central Sudan, Dataset Papers in Geosciences, 2013, 1–6, https://doi.org/10.7167/2013/297973, 2013.

AWST, TU Wien, CESBIO: QA4SM Software User Manual, Version 3.1, Tech. rep., QA4SM Consortium, 2025.

Bartalis, Z., Kidd, R. A., and Scipal, K.: Development and Implementation of a Discrete Global Grid System for Soil Moisture Retrieval Using the MetOp ASCAT Scatterometer, in: First EPS/MetOp RAO Workshop, Frascati, Italy, 15–17 May, eSA Special Publication SP-618, 2006a.

Bartalis, Z., Scipal, K., and Wagner, W.: Azimuthal Anisotropy of Scatterometer Measurements over Land, IEEE Transactions on Geoscience and Remote Sensing, 44, 2083–2092, 2006b.

Bartalis, Z., Wagner, W., Naeimi, V., Hasenauer, S., Scipal, K., Bonekamp, H., Figa, J., and Anderson, C.: Initial soil moisture retrievals from the METOP-A Advanced Scatterometer (ASCAT), Geophysical Research Letters, 34, https://doi.org/10.1029/2007gl031088, 2007.

Bauer-Marschallinger, B., Paulik, C., Hochstöger, S., Mistelbauer, T., Modanesi, S., Ciabatta, L., Massari, C., Brocca, L., and Wagner, W.: Soil Moisture from Fusion of Scatterometer and SAR: Closing the Scale Gap with Temporal Filtering, Remote Sensing, 10, 1030, https://doi.org/10.3390/rs10071030, 2018.

Beaudoing, H., Rodell, M., and NASA/GSFC/HSL: GLDAS Noah Land Surface Model L4 3 hourly 0.25 x 0.25 degree, Version 2.1, https://doi.org/10.5067/E7TYRXPJKWOQ, 2020.

Beck, H. E., Pan, M., Miralles, D. G., Reichle, R. H., Dorigo, W. A., Hahn, S., Sheffield, J., Karthikeyan, L., Balsamo, G., Parinussa, R. M., van Dijk, A. I. J. M., Du, J., Kimball, J. S., Vergopolan, N., and Wood, E. F.: Evaluation of 18 satellite- and model-based soil moisture products using in situ measurementsfrom 826 sensors, Hydrology and Earth System Sciences, 25, 17–40, https://doi.org/10.5194/hess-25-17-2021, 2021.

Bell, J. E., Palecki, M. A., Baker, C. B., Collins, W. G., Lawrimore, J. H., Leeper, R. D., Hall, M. E., Kochendorfer, J., Meyers, T. P., Wilson, T., and Diamond, H. J.: U.S. Climate Reference Network Soil Moisture and Temperature Observations, Journal of Hydrometeorology, 14, 977–988, https://doi.org/10.1175/jhm-d-12-0146.1, 2013.

Beyrich, F. and Adam, W.: Site and Data Report for the Lindenberg Reference Site in CEOP – Phase 1, Tech. Rep. 230, Deutscher Wetterdienst, Offenbach am Main, 2007.

Bircher, S., Balling, J. E., Skou, N., and Kerr, Y. H.: Validation of SMOS Brightness Temperatures During the HOBE Airborne Campaign, Western Denmark, IEEE Transactions on Geoscience and Remote Sensing, 50, 1468–1482, https://doi.org/10.1109/TGRS.2011.2170177, 2012.

Blöschl, G., Blaschke, A. P., Broer, M., Bucher, C., Carr, G., Chen, X., Eder, A., Exner-Kittridge, M., Farnleitner, A., Flores-Orozco, A., Haas, P., Hogan, P., Kazemi Amiri, A., Oismüller, M., Parajka, J., Silasari, R., Stadler, P., Strauss, P., Vreugdenhil, M., Wagner, W., and Zessner, M.: The Hydrological Open Air Laboratory (HOAL) in Petzenkirchen: a hypothesis-driven observatory, Hydrology and Earth System Sciences, 20, 227–255, https://doi.org/10.5194/hess-20-227-2016, 2016.

Bogena, H., Kunkel, R., Puetz, T., Vereecken, H., Krueger, E., Zacharias, S., Dietrich, P., Wollschlaeger, U., Kunstmann, H., and Papen, H.: Tereno-long-term monitoring network for terrestrial environmental research, Hydrologie und Wasserbewirtschaftung, 56, 138–143, 2012.

Bogena, H., Montzka, C., Huisman, J., Graf, A., Schmidt, M., Stockinger, M., von Hebel, C., Hendricks-Franssen, H., van der Kruk, J., Tappe, W., Lücke, A., Baatz, R., Bol, R., Groh, J., Pütz, T., Jakobi, J., Kunkel, R., Sorg, J., and Vereecken, H.: The TERENO-Rur Hydrological Observatory: A Multiscale Multi-Compartment Research Platform for the Advancement of Hydrological Science, Vadose Zone Journal, 17, 1–22, https://doi.org/10.2136/vzj2018.03.0055, 2018.

Bogena, H. R.: TERENO: German network of terrestrial environmental observatories, Journal of large-scale research facilities JLSRF, 2, A52, https://doi.org/10.17815/jlsrf-2-98, 2016.

Brocca, L., Melone, F., Moramarco, T., Wagner, W., Naeimi, V., Bartalis, Z., and Hasenauer, S.: Improving Runoff Prediction through the Assimilation of the ASCAT Soil Moisture Product, Hydrology and Earth System Sciences, 14, 1881–1893, https://doi.org/10.5194/hess-14-1881-2010, 2010.

Brocca, L., Moramarco, T., Melone, F., Wagner, W., Hasenauer, S., and Hahn, S.: Assimilation of Surface- and Root-Zone ASCAT Soil Moisture Products Into Rainfall-Runoff Modeling, IEEE Transactions on Geoscience and Remote Sensing, 50, 2542–2555, https://doi.org/10.1109/TGRS.2011.2177468, 2012.

Brocca, L., Moramarco, T., Melone, F., and Wagner, W.: A New Method for Rainfall Estimation through Soil Moisture Observations: RAINFALL FROM SOIL MOISTURE OBSERVATIONS, Geophysical Research Letters, 40, 853–858, https://doi.org/10.1002/grl.50173, 2013.

Brocca, L., Ciabatta, L., Massari, C., Moramarco, T., Hahn, S., Hasenauer, S., Kidd, R., Dorigo, W., Wagner, W., and Levizzani, V.: Soil as a Natural Rain Gauge: Estimating Global Rainfall from Satellite Soil Moisture Data: Using the Soil as a Natural Raingauge, Journal of Geophysical Research: Atmospheres, 119, 5128–5141, https://doi.org/10.1002/2014JD021489, 2014.

Brocca, L., Crow, W. T., Ciabatta, L., Massari, C., de Rosnay, P., Enenkel, M., Hahn, S., Amarnath, G., Camici, S., Tarpanelli, A., and Wagner, W.: A Review of the Applications of ASCAT Soil Moisture Products, IEEE Journal of Selected Topics in Applied Earth Observations and Remote Sensing, 10, 2285–2306, https://doi.org/10.1109/JSTARS.2017.2651140, 2017.

Brocca, L., Filippucci, P., Hahn, S., Ciabatta, L., Massari, C., Camici, S., Schüller, L., Bojkov, B., and Wagner, W.: SM2RAIN–ASCAT (2007–2018): global daily satellite rainfall data from ASCAT soil moisture observations, Earth System Science Data, 11, 1583–1601, https://doi.org/10.5194/essd-11-1583-2019, 2019.

Caldwell, T. G., Bongiovanni, T., Cosh, M. H., Jackson, T. J., Colliander, A., Abolt, C. J., Casteel, R., Larson, T., Scanlon, B. R., and Young, M. H.: The Texas Soil Observation Network:A Comprehensive Soil Moisture Dataset for Remote Sensing and Land Surface Model Validation, Vadose Zone Journal, 18, 1–20, https://doi.org/10.2136/vzj2019.04.0034, 2019.

Calvet, J.-C., Fritz, N., Froissard, F., Suquia, D., Petitpa, A., and Piguet, B.: In situ soil moisture observations for the CAL/VAL of SMOS: the SMOSMANIA network, in: 2007 IEEE International Geoscience and Remote Sensing Symposium, p. 1196–1199, IEEE, https://doi.org/10.1109/igarss.2007.4423019, 2007.

Calvet, J.-C., Fritz, N., Berne, C., Piguet, B., Maurel, W., and Meurey, C.: Deriving pedotransfer functions for soil quartz fraction in southern France from reverse modeling, SOIL, 2, 615–629, https://doi.org/10.5194/soil-2-615-2016, 2016.

Capello, G., Biddoccu, M., Ferraris, S., and Cavallo, E.: Effects of Tractor Passes on Hydrological and Soil Erosion Processes in Tilled and Grassed Vineyards, Water, 11, 2118, https://doi.org/10.3390/w11102118, 2019.

Cappelaere, B., Descroix, L., Lebel, T., Boulain, N., Ramier, D., Laurent, J.-P., Favreau, G., Boubkraoui, S., Boucher, M., Bouzou Moussa, I., Chaffard, V., Hiernaux, P., Issoufou, H., Le Breton, E., Mamadou, I., Nazoumou, Y., Oi, M., Ottlé, C., and Quantin, G.: The AMMA-CATCH experiment in the cultivated Sahelian area of south-west Niger – Investigating water cycle response to a fluctuating climate and changing environment, Journal of Hydrology, 375, 34–51, https://doi.org/10.1016/j.jhydrol.2009.06.021, 2009.

Chan, S., Bindlish, R., O'Neill, P., Jackson, T., Njoku, E., Dunbar, S., Chaubell, J., Piepmeier, J., Yueh, S., Entekhabi, D., Colliander, A., Chen, F., Cosh, M., Caldwell, T., Walker, J., Berg, A., McNairn, H., Thibeault, M., Martínez-Fernández, J., Uldall, F., Seyfried, M., Bosch, D., Starks, P., Holifield Collins, C., Prueger, J., van der Velde, R., Asanuma, J., Palecki, M., Small, E., Zreda, M., Calvet, J., Crow, W., and Kerr, Y.: Development and assessment of the SMAP enhanced passive soil moisture product, Remote Sensing of Environment, 204, 931–941, https://doi.org/10.1016/j.rse.2017.08.025, 2018.

Chan, S. K., Bindlish, R., O'Neill, P. E., Njoku, E., Jackson, T., Colliander, A., Chen, F., Burgin, M., Dunbar, S., Piepmeier, J., Yueh, S., Entekhabi, D., Cosh, M. H., Caldwell, T., Walker, J., Wu, X., Berg, A., Rowlandson, T., Pacheco, A., McNairn, H., Thibeault, M., Martinez-Fernandez, J., Gonzalez-Zamora, A., Seyfried, M., Bosch, D., Starks, P., Goodrich, D., Prueger, J., Palecki, M., Small, E. E., Zreda, M., Calvet, J.-C., Crow, W. T., and Kerr, Y.: Assessment of the SMAP Passive Soil Moisture Product, IEEE Transactions on Geoscience and Remote Sensing, 54, 4994–5007, https://doi.org/10.1109/tgrs.2016.2561938, 2016.

Cook, D. R.: Soil temperature and moisture profile (STAMP) system handbook, Technical report, DOE Office of Science Atmospheric Radiation Measurement (ARM) Program, https://www.osti.gov/biblio/1332724, 2016a.

Cook, D. R.: Soil water and temperature system (SWATS) instrument handbook, Technical report, DOE Office of Science Atmospheric Radiation Measurement (ARM) Program, https://www.osti.gov/biblio/1004944, 2016b.

Cooper, H. M., Bennett, E., Blake, J., Blyth, E., Boorman, D., Cooper, E., Evans, J., Fry, M., Jenkins, A., Morrison, R., Rylett, D., Stanley, S., Szczykulska, M., Trill, E., Antoniou, V., Askquith-Ellis, A., Ball, L., Brooks, M., Clarke, M. A., Cowan, N., Cumming, A., Farrand, P., Hitt, O., Lord, W., Scarlett, P., Swain, O., Thornton, J., Warwick, A., and Winterbourn, B.: COSMOS-UK: national soil moisture and hydrometeorology data for environmental science research, Earth System Science Data, 13, 1737–1757, https://doi.org/10.5194/essd-13-1737-2021, 2021.

Copernicus: Copernicus DEM, https://doi.org/10.5270/ESA-c5d3d65, 2021.

Copernicus Climate Change Service: Soil moisture gridded data from 1978 to present, https://doi.org/10.24381/CDS.D7782F18, 2018.

Darouich, H., Ramos, T. B., Pereira, L. S., Rabino, D., Bagagiolo, G., Capello, G., Simionesei, L., Cavallo, E., and Biddoccu, M.: Water Use and Soil Water Balance of Mediterranean Vineyards under Rainfed and Drip Irrigation Management: Evapotranspiration Partition and Soil Management Modelling for Resource Conservation, Water, 14, 554, https://doi.org/10.3390/w14040554, 2022.

de Rosnay, P., Gruhier, C., Timouk, F., Baup, F., Mougin, E., Hiernaux, P., Kergoat, L., and LeDantec, V.: Multi-Scale Soil Moisture Measurements at the Gourma Meso-Scale Site in Mali, Journal of Hydrology, 375, 241–252, https://doi.org/10.1016/j.jhydrol.2009.01.015, 2009.

Dente, L., Vekerdy, Z., Wen, J., and Su, Z.: Maqu Network for Validation of Satellite-Derived Soil Moisture Products, International Journal of Applied Earth Observation and Geoinformation, 17, 55–65, https://doi.org/10.1016/j.jag.2011.11.004, 2012.

Dharssi, I., Bovis, K. J., Macpherson, B., and Jones, C. P.: Operational assimilation of ASCAT surface soil wetness at the Met Office, Hydrology and Earth System Sciences, 15, 2729–2746, https://doi.org/10.5194/hess-15-2729-2011, 2011.

Dorigo, W., Wagner, W., Albergel, C., Albrecht, F., Balsamo, G., Brocca, L., Chung, D., Ertl, M., Forkel, M., Gruber, A., Haas, E., Hamer, P. D., Hirschi, M., Ikonen, J., de Jeu, R., Kidd, R., Lahoz, W., Liu, Y. Y., Miralles, D., Mistelbauer, T., Nicolai-Shaw, N., Parinussa, R., Pratola, C., Reimer, C., van der Schalie, R., Seneviratne, S. I., Smolander, T., and Lecomte, P.: ESA CCI Soil Moisture for improved Earth system understanding: State-of-the art and future directions, Remote Sensing of Environment, 203, 185–215, https://doi.org/10.1016/j.rse.2017.07.001, 2017.

Dorigo, W., Himmelbauer, I., Aberer, D., Schremmer, L., Petrakovic, I., Zappa, L., Preimesberger, W., Xaver, A., Annor, F., Ardö, J., Baldocchi, D., Blöschl, G., Bogena, H., Brocca, L., Calvet, J.-C., Camarero, J. J., Capello, G., Choi, M., Cosh, M. C., Demarty, J., van de Giesen, N., Hajdu, I., Jensen, K. H., Kanniah, K. D., de Kat, I., Kirchengast, G., Kyrouac, P. K. R. J., Larson, K., Liu, S., Loew, A., Moghaddam, M., Fernández, J. M., Bader, C. M., Morbidelli, R., Musial, J. P., Osenga, E., Palecki, M. A., Pfeil, I., Powers, J., Ikonen, J., Robock, A., Rüdiger, C., Rummel, U., Strobel, M., Su, Z., Sullivan, R., Tagesson, T., Vreugdenhil, M., Walker, J., Wigneron, J. P., Woods, M., Yang, K., Zhang, X., Zreda, M., Dietrich, S., Gruber, A., van Oevelen, P., Wagner, W., Scipal, K., Drusch, M., and Sabia, R.: The International Soil Moisture Network: serving Earth system science for over a decade, Hydrology and Earth System Sciences, https://doi.org/10.5194/hess-2021-2, 2021.

Dorigo, W. A., Wagner, W., Hohensinn, R., Hahn, S., Paulik, C., Xaver, A., Gruber, A., Drusch, M., Mecklenburg, S., van Oevelen, P., Robock, A., and Jackson, T.: The International Soil Moisture Network: A Data Hosting Facility for Global in Situ Soil Moisture Measurements, Hydrology and Earth System Sciences, 15, 1675–1698, https://doi.org/10.5194/hess-15-1675-2011, 2011.

Draper, C., Mahfouf, J.-F., Calvet, J.-C., Martin, E., and Wagner, W.: Assimilation of ASCAT near-surface soil moisture into the SIM hydrological model over France, Hydrology and Earth System Sciences, 15, 3829–3841, https://doi.org/10.5194/hess-15-3829-2011, 2011.

Draper, C. S., Reichle, R. H., Lannoy, G. J. M. D., and Liu, Q.: Assimilation of passive and active microwave soil moisture retrievals, Geophysical Research Letters, 39, n/a–n/a, https://doi.org/10.1029/2011gl050655, 2012.

Eaton, B., Gregory, J., Drach, B., Taylor, K., Hankin, S., Caron, J., Signell, R., Bentley, P., Rappa, G., Höck, H., Pamment, A., Juckes, M., Raspaud, M., Blower, J., Horne, R., Whiteaker, T., Blodgett, D., Zender, C., Lee, D., Hassell, D., Snow, A. D., Kölling, T., Allured, D., Jelenak, A., Soerensen, A. M., Gaultier, L., Herlédan, S., Manzano, F., Bärring, L., Barker, C., and Bartholomew, S. L.: NetCDF Climate and Forecast (CF) Metadata Conventions, https://doi.org/10.5281/ZENODO.14275599, 2024.

ESA: Land Cover CCI Product User Guide Version 2.0, European Space Agency, available at: http://maps.elie.ucl.ac.be/CCI/viewer/download/ESACCI-LC-Ph2-PUGv2_2.0.pdf (last access: 12 July 2025), 2017.

European Space Agency: SMOS L2 SM V700, https://doi.org/10.57780/SM1-857C3D7, 2021.

https://doi.org/10.5194/essd-2025-746
Preprint. Discussion started: 2 February 2026

Fan, X., Lu, Y., Liu, Y., Li, T., Xun, S., and Zhao, X.: Validation of Multiple Soil Moisture Products over an Intensive Agricultural Region: Overall Accuracy and Diverse Responses to Precipitation and Irrigation Events, Remote Sensing, 14, 3339, https://doi.org/10.3390/rs14143339, 2022.

Fascetti, F., Pierdicca, N., Pulvirenti, L., Crapolicchio, R., and Muñoz-Sabater, J.: A Comparison of ASCAT and SMOS Soil Moisture Retrievals over Europe and Northern Africa from 2010 to 2013, International Journal of Applied Earth Observation and Geoinformation, 45, 135–142, https://doi.org/10.1016/j.jag.2015.09.008, 2016.

Figa-Saldana, J., Wilson, J. J. W., Attema, E., Gelsthorpe, R., Drinkwater, M. R., and Stoffelen, A.: The Advanced Scatterometer (ASCAT) on the Meteorological Operational (MetOp) Platform: A Follow on for European Wind Scatterometers, Canadian Journal of Remote Sensing, 28, 404–412, https://doi.org/10.5589/m02-035, 2002.

Galle, S., Grippa, M., Peugeot, C., Bouzou Moussa, I., Cappelaere, B., Demarty, J., Mougin, E., Lebel, T., and Chaffard, V.: AMMA-CATCH: a Hydrological, Meteorological and Ecological Long Term Observatory on West Africa: Some Recent Results, in: AGU Fall Meeting Abstracts, vol. 2015, pp. GC42A–01, 2015.

Gaona, J., Bavera, D., Fioravanti, G., Hahn, S., Stradiotti, P., Filippucci, P., Camici, S., Ciabatta, L., Mosaffa, H., Puca, S., Roberto, N., and Brocca, L.: Soil moisture product consistency for operational drought monitoring in Europe, Hydrology and Earth System Sciences, 29, 3865–3888, https://doi.org/10.5194/hess-29-3865-2025, 2025.

Gelsthorpe, R. V., Schied, E., and Wilson, J. J. W.: ASCAT – Metop's Advanced Scatterometer, ESA Bulletin (ISSN 0376-4265), 102, 19–27, 2000.

Gómez, B., Charlton-Pérez, C. L., Lewis, H., and Candy, B.: The Met Office Operational Soil Moisture Analysis System, Remote Sensing, 12, 3691, https://doi.org/10.3390/rs12223691, 2020.

González-Zamora, Á., Sánchez, N., Pablos, M., and Martínez-Fernández, J.: CCI soil moisture assessment with SMOS soil moisture and in situ data under different environmental conditions and spatial scales in Spain, Remote Sensing of Environment, 225, 469–482, https://doi.org/10.1016/j.rse.2018.02.010, 2019.

Gruber, A., Su, C.-H., Zwieback, S., Crow, W., Dorigo, W., and Wagner, W.: Recent Advances in (Soil Moisture) Triple Collocation Analysis, International Journal of Applied Earth Observation and Geoinformation, 45, 200–211, https://doi.org/10.1016/j.jag.2015.09.002, 2016.

Gruber, A., Scanlon, T., van der Schalie, R., Wagner, W., and Dorigo, W.: Evolution of the ESA CCI Soil Moisture climate data records and their underlying merging methodology, Earth System Science Data, 11, 717–739, https://doi.org/10.5194/essd-11-717-2019, 2019.

H SAF: Metop ASCAT Surface Soil Moisture Climate Data Record v4 12.5 km sampling (ASCAT SSM CDR v4 12.5 km - H115), https://doi.org/10.15770/EUM_SAF_H_0004, EUMETSAT SAF on Support to Operational Hydrology and Water Management, 2017.

H SAF: Metop ASCAT Surface Soil Moisture Climate Data Record v5 12.5 km sampling (ASCAT SSM CDR v5 12.5 km - H115), https://doi.org/10.15770/EUM_SAF_H_0006, EUMETSAT SAF on Support to Operational Hydrology and Water Management, 2020.

H SAF: Metop ASCAT Surface Soil Moisture Climate Data Record v7 12.5 km sampling (ASCAT SSM CDR v7 12.5 km - H119), https://doi.org/10.15770/EUM_SAF_H_0009, EUMETSAT SAF on Support to Operational Hydrology and Water Management, 2021.

H SAF: Metop ASCAT Surface Soil Moisture Climate Data Record v8 12.5 km sampling (ASCAT SSM CDR v8 12.5 km - H121), https://doi.org/10.15770/EUM_SAF_H_0011, EUMETSAT SAF on Support to Operational Hydrology and Water Management, 2025a.

H SAF: Metop ASCAT Surface Soil Moisture Near Real Time 6.25 km sampling (ASCAT SSM NRT 6.25 km - H122), EUMETSAT SAF on Support to Operational Hydrology and Water Management, 2025b.

H SAF: Metop ASCAT Surface Soil Moisture Climate Data Record v1 6.25 km sampling (ASCAT SSM CDR v1 6.25 km - H129), https://doi.org/10.15770/EUM_SAF_H_0012, EUMETSAT SAF on Support to Operational Hydrology and Water Management, 2025c.

https://doi.org/10.5194/essd-2025-746
Preprint. Discussion started: 2 February 2026

H SAF: Metop ASCAT Surface Soil Moisture Near Real Time 12.5 km sampling (ASCAT SSM NRT v2 12.5 km - H29), EUMETSAT SAF on Support to Operational Hydrology and Water Management, 2025d.

Hahn, S., Reimer, C., Vreugdenhil, M., Melzer, T., and Wagner, W.: Dynamic Characterization of the Incidence Angle Dependence of Backscatter Using Metop ASCAT, IEEE Journal of Selected Topics in Applied Earth Observations and Remote Sensing, 10, 2348–2359, https://doi.org/10.1109/jstars.2016.2628523, 2017.

Hahn, S., Wagner, W., Steele-Dunne, S. C., Vreugdenhil, M., and Melzer, T.: Improving ASCAT Soil Moisture Retrievals With an Enhanced Spatially Variable Vegetation Parameterization, IEEE Transactions on Geoscience and Remote Sensing, 59, 8241–8256, https://doi.org/10.1109/tgrs.2020.3041340, 2021.

Hahn, S., Harrison, C., Paulik, C., Preimesberger, W., and Schmitzer, M.: TUW-GEO/ascat: v2.6.5, https://doi.org/10.5281/ZENODO.16083028, 2025.

Hallikainen, M., Ulaby, F., Dobson, M., El-rayes, M., and Wu, L.-k.: Microwave Dielectric Behavior of Wet Soil-Part 1: Empirical Models and Experimental Observations, IEEE Transactions on Geoscience and Remote Sensing, GE-23, 25–34, https://doi.org/10.1109/TGRS.1985.289497, 1985.

Hallikainen, M., Ulaby, F., and Abdelrazik, M.: Dielectric Properties of Snow in the 3 to 37 GHz Range, IEEE Transactions on Antennas and Propagation, 34, 1329–1340, https://doi.org/10.1109/TAP.1986.1143757, 1986.

Ikonen, J., Vehviläinen, J., Rautiainen, K., Smolander, T., Lemmetyinen, J., Bircher, S., and Pulliainen, J.: The Sodankylä in situ soil moisture observation network: an example application of ESA CCI soil moisture product evaluation, Geoscientific Instrumentation, Methods and Data Systems, 5, 95–108, https://doi.org/10.5194/gi-5-95-2016, 2016.

Jensen, K. H. and Refsgaard, J. C.: HOBE: The Danish Hydrological Observatory, Vadose Zone Journal, 17, 1–24, https://doi.org/10.2136/vzj2018.03.0059, 2018.

Kim, D., Lee, S., Cho, S., Kim, D., and Choi, M.: Evaluating rainfall estimates derived from soil moisture using soil hydraulic properties over the Korean Peninsula, Journal of Hydrology, 663, 134 267, https://doi.org/10.1016/j.jhydrol.2025.134267, 2025.

Kim, H., Crow, W., Li, X., Wagner, W., Hahn, S., and Lakshmi, V.: True global error maps for SMAP, SMOS, and ASCAT soil moisture data based on machine learning and triple collocation analysis, Remote Sensing of Environment, 298, 113 776, https://doi.org/10.1016/j.rse.2023.113776, 2023.

Land Product Validation Subgroup (Working Group On Calibration And Validation Committee On Earth Observation Satellites): Soil Moisture Product Validation Good Practices Protocol, https://doi.org/10.5067/DOC/CEOSWGCV/LPV/SM.001, 2020.

Leavesley, G., David, O., Garen, D., Lea, J., Marron, J., Pagano, T., Perkins, T., and Strobel, M.: A Modeling Framework for Improved Agricultural Water Supply Forecasting, AGU Fall Meeting Abstracts, 2008.

Lebel, T., Cappelaere, B., Galle, S., Hanan, N., Kergoat, L., Levis, S., Vieux, B., Descroix, L., Gosset, M., Mougin, E., Peugeot, C., and Seguis, L.: AMMA-CATCH studies in the Sahelian region of West-Africa: An overview, Journal of Hydrology, 375, 3–13, https://doi.org/10.1016/j.jhydrol.2009.03.020, 2009.

Lehner, B. and Döll, P.: Development and Validation of a Global Database of Lakes, Reservoirs and Wetlands, Journal of Hydrology, 296, 1–22, https://doi.org/10.1016/j.jhydrol.2004.03.028, 2004.

Lindorfer, R., Wagner, W., Hahn, S., Kim, H., Vreugdenhil, M., Gruber, A., Fischer, M., and Trnka, M.: Global Scale Maps of Subsurface Scattering Signals Impacting ASCAT Soil Moisture Retrievals, https://doi.org/10.48436/54SHJ-JZQ57, 2023.

Lindsley, R. D., Anderson, C., Figa-Saldana, J., and Long, D. G.: A Parameterized ASCAT Measurement Spatial Response Function, IEEE Transactions on Geoscience and Remote Sensing, pp. 1–10, https://doi.org/10.1109/TGRS.2016.2544835, 2016.

https://doi.org/10.5194/essd-2025-746
Preprint. Discussion started: 2 February 2026

Loew, A., Bell, W., Brocca, L., Bulgin, C. E., Burdanowitz, J., Calbet, X., Donner, R. V., Ghent, D., Gruber, A., Kaminski, T., Kinzel, J., Klepp, C., Lambert, J.-C., Schaepman-Strub, G., Schröder, M., and Verhoelst, T.: Validation practices for satellite-based Earth observation data across communities, Reviews of Geophysics, 55, 779–817, https://doi.org/10.1002/2017rg000562, 2017.

Marczewski, W., Slominski, J., Slominska, E., Usowicz, B., Usowicz, J., Romanov, S., Maryskevych, O., Nastula, J., and Zawadzki, J.: Strategies for validating and directions for employing SMOS data, in the Cal-Val project SWEX (3275) for wetlands, https://doi.org/10.5194/hessd-7-7007-2010, 2010.

Mattar, C., Santamaría-Artigas, A., Durán-Alarcón, C., Olivera-Guerra, L., and Fuster, R.: LAB-net: the first Chilean soil moisture network for remote sensing applications, in: Quantitative Remote Sensing Symposium (RAQRS), pp. 22–26, 2014.

Mattar, C., Santamaría-Artigas, A., Durán-Alarcón, C., Olivera-Guerra, L., Fuster, R., and Borvarán, D.: The LAB-Net Soil Moisture Network: Application to Thermal Remote Sensing and Surface Energy Balance, Data, 1, 6, https://doi.org/10.3390/data1010006, 2016.

Mazzariello, A., Albano, R., Lacava, T., Manfreda, S., and Sole, A.: Intercomparison of recent microwave satellite soil moisture products on European ecoregions, Journal of Hydrology, 626, 130 311, https://doi.org/10.1016/j.jhydrol.2023.130311, 2023.

Melzer, T.: Vegetation Modelling in WARP 6.0, in: EUMETSAT Meteorological Satellite Conference, Vienna, Austria, 2013.

Moghaddam, M., Entekhabi, D., Goykhman, Y., Li, K., Liu, M., Mahajan, A., Nayyar, A., Shuman, D., and Teneketzis, D.: A Wireless Soil Moisture Smart Sensor Web Using Physics-Based Optimal Control: Concept and Initial Demonstrations, IEEE Journal of Selected Topics in Applied Earth Observations and Remote Sensing, 3, 522–535, https://doi.org/10.1109/jstars.2010.2052918, 2010.

Moghaddam, M., Silva, A., Clewley, D., Akbar, R., Hussaini, S., Whitcomb, J., Devarakonda, R., Shrestha, R., Cook, R., Prakash, G., Santhana Vannan, S., and Boyer, A.: Soil Moisture Profiles and Temperature Data from SoilSCAPE Sites, USA, https://doi.org/10.3334/ORNLDAAC/1339, 2016.

Morrison, K. and Wagner, W.: Explaining Anomalies in SAR and Scatterometer Soil Moisture Retrievals From Dry SoilsWith Subsurface Scattering, IEEE Transactions on Geoscience and Remote Sensing, 58, 2190–2197, https://doi.org/10.1109/tgrs.2019.2954771, 2020.

Mougin, E., Hiernaux, P., Kergoat, L., Grippa, M., de Rosnay, P., Timouk, F., Le Dantec, V., Demarez, V., Lavenu, F., Arjounin, M., Lebel, T., Soumaguel, N., Ceschia, E., Mougenot, B., Baup, F., Frappart, F., Frison, P., Gardelle, J., Gruhier, C., Jarlan, L., Mangiarotti, S., Sanou, B., Tracol, Y., Guichard, F., Trichon, V., Diarra, L., Soumaré, A., Koité, M., Dembélé, F., Lloyd, C., Hanan, N., Damesin, C., Delon, C., Serça, D., Galy-Lacaux, C., Seghieri, J., Becerra, S., Dia, H., Gangneron, F., and Mazzega, P.: The AMMA-CATCH Gourma observatory site in Mali: Relating climatic variations to changes in vegetation, surface hydrology, fluxes and natural resources, Journal of Hydrology, 375, 14–33, https://doi.org/10.1016/j.jhydrol.2009.06.045, 2009.

Naeimi, V., Bartalis, Z., and Wagner, W.: ASCAT Soil Moisture: An Assessment of the Data Quality and Consistency with the ERS Scatterometer Heritage, Journal of Hydrometeorology, 10, 555–563, https://doi.org/10.1175/2008JHM1051.1, 2009a.

Naeimi, V., Scipal, K., Bartalis, Z., Hasenauer, S., and Wagner, W.: An Improved Soil Moisture Retrieval Algorithm for ERS and METOP Scatterometer Observations, IEEE Transactions on Geoscience and Remote Sensing, 47, 1999–2013, https://doi.org/10.1109/tgrs.2008.2011617, 2009b.

Nguyen, H. H., Kim, H., and Choi, M.: Evaluation of the soil water content using cosmic-ray neutron probe in a heterogeneous monsoon climate-dominated region, Advances in Water Resources, 108, 125–138, https://doi.org/10.1016/j.advwatres.2017.07.020, 2017.

Ojo, E. R., Bullock, P. R., L'Heureux, J., Powers, J., McNairn, H., and Pacheco, A.: Calibration and Evaluation of a Frequency Domain Reflectometry Sensor for Real-Time Soil Moisture Monitoring, Vadose Zone Journal, 14, 1–12, https://doi.org/10.2136/vzj2014.08.0114, 2015.

https://doi.org/10.5194/essd-2025-746
Preprint. Discussion started: 2 February 2026

Open Access Earth System Science Data Discussions

ONeill, P., Chan, S., Njoku, E., Jackson, T., Bindlish, R., and Chaubell, J.: SMAP L2 Radiometer Half-Orbit 36 km EASE-Grid Soil Moisture, Version 9, https://doi.org/10.5067/K7Y2D8QQVZ4L, 2023a.

ONeill, P., Chan, S., Njoku, E., Jackson, T., Bindlish, R., Chaubell, J., and Colliander, A.: SMAP Enhanced L2 Radiometer Half-Orbit 9 km EASE-Grid Soil Moisture, Version 6, https://doi.org/10.5067/BN36FXOMMC4C, 2023b.

Owe, M., de Jeu, R., and Holmes, T.: Multisensor Historical Climatology of Satellite-Derived Global Land Surface Moisture, Journal of Geophysical Research, 113, https://doi.org/10.1029/2007JF000769, 2008.

Paulik, C., Dorigo, W., Wagner, W., and Kidd, R.: Validation of the ASCAT Soil Water Index Using in Situ Data from the International Soil Moisture Network, International Journal of Applied Earth Observation and Geoinformation, 30, 1–8, https://doi.org/10.1016/j.jag.2014.01.007, 2014.

Peel, M. C., Finlayson, B. L., and McMahon, T. A.: Updated World Map of the Köppen-Geiger Climate Classification, Hydrology and Earth System Sciences, 11, 1633–1644, https://doi.org/10.5194/hess-11-1633-2007, 2007.

Pellarin, T., Laurent, J., Cappelaere, B., Decharme, B., Descroix, L., and Ramier, D.: Hydrological Modelling and Associated Microwave Emission of a Semi-Arid Region in South-Western Niger, Journal of Hydrology, 375, 262–272, https://doi.org/10.1016/j.jhydrol.2008.12.003, 2009.

Petropoulos, G. and McCalmont, J.: An Operational In Situ Soil Moisture and Soil Temperature Monitoring Network for West Wales, UK: The WSMN Network, Sensors, 17, 1481, https://doi.org/10.3390/s17071481, 2017.

Rodell, M., Houser, P. R., Jambor, U., Gottschalck, J., Mitchell, K., Meng, C.-J., Arsenault, K., Cosgrove, B., Radakovich, J., Bosilovich, M., Entin*, J. K., Walker, J. P., Lohmann, D., and Toll, D.: The Global Land Data Assimilation System, Bulletin of the American Meteorological Society, 85, 381–394, https://doi.org/10.1175/BAMS-85-3-381, 2004.

Rodríguez-Fernández, N. J., Sabater, J. M., Richaume, P., de Rosnay, P., Kerr, Y. H., Albergel, C., Drusch, M., and Mecklenburg, S.: SMOS near-real-time soil moisture product: processor overview and first validation results, Hydrology and Earth System Sciences, 21, 5201–5216, https://doi.org/10.5194/hess-21-5201-2017, 2017.

Rüdiger, C., Hancock, G., Hemakumara, H. M., Jacobs, B., Kalma, J. D., Martinez, C., Thyer, M., Walker, J. P., Wells, T., and Willgoose, G. R.: Goulburn River experimental catchment data set, Water Resources Research, 43, https://doi.org/10.1029/2006wr005837, 2007.

Schaefer, G. L., Cosh, M. H., and Jackson, T. J.: The USDA Natural Resources Conservation Service Soil Climate Analysis Network (SCAN), Journal of Atmospheric and Oceanic Technology, 24, 2073–2077, https://doi.org/10.1175/2007jtecha930.1, 2007.

Scipal, K., Wagner, W., Trommler, M., and Naumann, K.: The Global Soil Moisture Archive 1992-2000 from ERS Scatterometer Data: First Results, in: IEEE International Geoscience and Remote Sensing Symposium, vol. 3, pp. 1399–1401, IEEE International Geoscience and Remote Sensing Symposium (IGARSS), Toronto, Canada, ISBN 0-7803-7536-X, https://doi.org/10.1109/IGARSS.2002.1026129, 2002.

Seo, E., Lee, M.-I., and Reichle, R. H.: Assimilation of SMAP and ASCAT soil moisture retrievals into the JULES land surface model using the Local Ensemble Transform Kalman Filter, Remote Sensing of Environment, 253, 112 222, https://doi.org/10.1016/j.rse.2020.112222, 2021.

Shuman, D. I., Nayyar, A., Mahajan, A., Goykhman, Y., Li, K., Liu, M., Teneketzis, D., Moghaddam, M., and Entekhabi, D.: Measurement Scheduling for Soil Moisture Sensing: From Physical Models to Optimal Control, Proceedings of the IEEE, 98, 1918–1933, https://doi.org/10.1109/jproc.2010.2052532, 2010.

Smith, A. B., Walker, J. P., Western, A. W., Young, R. I., Ellett, K. M., Pipunic, R. C., Grayson, R. B., Siriwardena, L., Chiew, F. H. S., and Richter, H.: The Murrumbidgee Soil Moisture Monitoring Network Data Set, Water Resources Research, 48, https://doi.org/10.1029/2012WR011976, 2012.

Steele-Dunne, S. C., Hahn, S., Wagner, W., and Vreugdenhil, M.: Investigating vegetation water dynamics and drought using Metop ASCAT over the North American Grasslands, Remote Sensing of Environment, 224, 219–235, https://doi.org/10.1016/j.rse.2019.01.004, 2019.

Steele-Dunne, S. C., Hahn, S., Wagner, W., and Vreugdenhil, M.: Towards Including Dynamic Vegetation Parameters in the EUMETSAT H SAF ASCAT Soil Moisture Products, Remote Sensing, 13, 1463, https://doi.org/10.3390/rs13081463, 2021.

Stephen, H. and Long, D.: Azimuth Modulation of Backscatter from SeaWinds and ERS Scatterometers over the Saharo-Arabian Deserts, in: IEEE International Geoscience and Remote Sensing Symposium, vol. 5, pp. 2808–2810, IEEE International Geoscience and Remote Sensing Symposium (IGARSS), Toronto, Canada, ISBN 0-7803-7536-X, https://doi.org/10.1109/IGARSS.2002.1026782, 2002.

Stoffelen, A.: Toward the True Near-Surface Wind Speed: Error Modeling and Calibration Using Triple Collocation, Journal of Geophysical Research, 103, 7755, https://doi.org/10.1029/97JC03180, 1998.

Su, Z., Wen, J., Dente, L., van der Velde, R., Wang, L., Ma, Y., Yang, K., and Hu, Z.: The Tibetan Plateau observatory of plateau scale soil moisture and soil temperature (Tibet-Obs) for quantifying uncertainties in coarse resolution satellite and model products, Hydrology and Earth System Sciences, 15, 2303–2316, https://doi.org/10.5194/hess-15-2303-2011, 2011.

Tagesson, T., Fensholt, R., Guiro, I., Rasmussen, M. O., Huber, S., Mbow, C., Garcia, M., Horion, S., Sandholt, I., Holm-Rasmussen, B., Göttsche, F. M., Ridler, M., Olén, N., Lundegard Olsen, J., Ehammer, A., Madsen, M., Olesen, F. S., and Ardö, J.: Ecosystem properties of semiarid savanna grassland in West Africa and its relationship with environmental variability, Global Change Biology, 21, 250–264, https://doi.org/10.1111/gcb.12734, 2014.

Ulaby, F. T., Moore, R. K., and Fung, A. K.: Microwave Remote Sensing: Active and Passive. Vol. II – Radar Remote Sensing and Surface Scattering and Emission Theory, Addison-Wesley, Advanced Book Program, Reading, MA, USA, 1982.

Ulaby, F. T., Moore, R. K., and Fung, A. K.: Microwave Remote Sensing: Active and Passive. Vol. III – Volume Scattering and Emission Theory, Advanced Systems and Applications, Artech House, Inc., Dedham, MA, USA, 1986.

van der Velde, R., Benninga, H.-J. F., Retsios, B., Vermunt, P. C., and Salama, M. S.: Twelve years of profile soil moisture and temperature measurements in Twente, the Netherlands, Earth System Science Data, 15, 1889–1910, https://doi.org/10.5194/essd-15-1889-2023, 2023.

Vogelzang, J., Stoffelen, A., Lindsley, R. D., Verhoef, A., and Verspeek, J.: The ASCAT 6.25-km Wind Product, IEEE Journal of Selected Topics in Applied Earth Observations and Remote Sensing, 10, 2321–2331, https://doi.org/10.1109/jstars.2016.2623862, 2017.

Vreugdenhil, M., Dorigo, W., Broer, M., Haas, P., Eder, A., Hogan, P., Bloeschl, G., and Wagner, W.: Towards a high-density soil moisture network for the validation of SMAP in Petzenkirchen, Austria, in: 2013 IEEE International Geoscience and Remote Sensing Symposium - IGARSS, p. 1865–1868, IEEE, https://doi.org/10.1109/igarss.2013.6723166, 2013.

Vreugdenhil, M., Hahn, S., Melzer, T., Bauer-Marschallinger, B., Reimer, C., Dorigo, W. A., and Wagner, W.: Assessing Vegetation Dynamics Over Mainland Australia With Metop ASCAT, IEEE Journal of Selected Topics in Applied Earth Observations and Remote Sensing, 10, 2240–2248, https://doi.org/10.1109/JSTARS.2016.2618838, 2017.

Wagner, W., Lemoine, G., Borgeaud, M., and Rott, H.: A study of vegetation cover effects on ERS scatterometer data, IEEE Transactions on Geoscience and Remote Sensing, 37, 938–948, https://doi.org/10.1109/36.752212, 1999a.

Wagner, W., Lemoine, G., and Rott, H.: A Method for Estimating Soil Moisture from ERS Scatterometer and Soil Data, Remote Sensing of Environment, 70, 191–207, https://doi.org/10.1016/S0034-4257(99)00036-X, 1999b.

Wagner, W., Noll, J., Borgeaud, M., and Rott, H.: Monitoring soil moisture over the Canadian Prairies with the ERS scatterometer, IEEE Transactions on Geoscience and Remote Sensing, 37, 206–216, https://doi.org/10.1109/36.739155, 1999c.

Wagner, W., Hahn, S., Kidd, R., Melzer, T., Bartalis, Z., Hasenauer, S., Figa-Saldaña, J., de Rosnay, P., Jann, A., Schneider, S., Komma, J., Kubu, G., Brugger, K., Aubrecht, C., Züger, J., Gangkofner, U., Kienberger, S., Brocca, L., Wang, Y., Blöschl, G., Eitzinger, J., Steinnocher, K., Zeil, P., and Rubel, F.: The ASCAT Soil Moisture Product: A Review of Its Specifications, Validation Results, and Emerging Applications, Meteorologische Zeitschrift, 22, 5–33, https://doi.org/10.1127/0941-2948/2013/0399, 2013.

Wagner, W., Lindorfer, R., Melzer, T., Hahn, S., Bauer-Marschallinger, B., Morrison, K., Calvet, J.-C., Hobbs, S., Quast, R., Greimeister-Pfeil, I., and Vreugdenhil, M.: Widespread occurrence of anomalous C-band backscatter signals in arid environments caused by subsurface scattering, Remote Sensing of Environment, 276, 113 025, https://doi.org/10.1016/j.rse.2022.113025, 2022.

Wagner, W., Lindorfer, R., Hahn, S., Kim, H., Vreugdenhil, M., Gruber, A., Fischer, M., and Trnka, M.: Global Scale Mapping of Subsurface Scattering Signals Impacting ASCAT Soil Moisture Retrievals, IEEE Transactions on Geoscience and Remote Sensing, 62, 1–20, https://doi.org/10.1109/tgrs.2024.3429550, 2024.

Wanders, N., Karssenberg, D., de Roo, A., de Jong, S. M., and Bierkens, M. F. P.: The Suitability of Remotely Sensed Soil Moisture for Improving Operational Flood Forecasting, Hydrology and Earth System Sciences, 18, 2343–2357, https://doi.org/10.5194/hess-18-2343-2014, 2014.

Wigneron, J.-P., Dayan, S., Kruszewski, A., Aluome, C., AI-Yaari, M. G.-E. A., Fan, L., Guven, S., Chipeaux, C., Moisy, C., Guyon, D., and Loustau, D.: The Aqui Network: Soil Moisture Sites in the “Les Landes” Forest and Graves Vineyards (Bordeaux Aquitaine Region, France), in: IGARSS 2018 - 2018 IEEE International Geoscience and Remote Sensing Symposium, p. 3739–3742, IEEE, https://doi.org/10.1109/igarss.2018.8517392, 2018.

Wismann, V.: Monitoring of seasonal thawing in Siberia with ERS scatterometer data, IEEE Transactions on Geoscience and Remote Sensing, 38, 1804–1809, https://doi.org/10.1109/36.851764, 2000.

Xie, Q., Jia, L., Menenti, M., Chen, Q., Bi, J., Chen, Y., Wang, C., and Yu, X.: Evaluation of remote sensing soil moisture data products with a new approach to analyse footprint mismatch with in-situ measurements, International Journal of Digital Earth, 17, https://doi.org/10.1080/17538947.2024.2437051, 2024.

Yang, K., Qin, J., Zhao, L., Chen, Y., Tang, W., Han, M., Lazhu, Chen, Z., Lv, N., Ding, B., Wu, H., and Lin, C.: A Multiscale Soil Moisture and Freeze–Thaw Monitoring Network on the Third Pole, Bulletin of the American Meteorological Society, 94, 1907–1916, https://doi.org/10.1175/bams-d-12-00203.1, 2013.

Young, R., Walker, J., Yeoh, N., Smith, A., Ellett, K., Merlin, O., and Western, A.: Soil moisture and meteorological observations from the Murrumbidgee catchment, Department of Civil and Environmental Engineering, The University of Melbourne, 2008.

Zacharias, S., Bogena, H., Samaniego, L., Mauder, M., Fuß, R., Pütz, T., Frenzel, M., Schwank, M., Baessler, C., Butterbach-Bahl, K., Bens, O., Borg, E., Brauer, A., Dietrich, P., Hajnsek, I., Helle, G., Kiese, R., Kunstmann, H., Klotz, S., Munch, J. C., Papen, H., Priesack, E., Schmid, H. P., Steinbrecher, R., Rosenbaum, U., Teutsch, G., and Vereecken, H.: A Network of Terrestrial Environmental Observatories in Germany, Vadose Zone Journal, 10, 955–973, https://doi.org/10.2136/vzj2010.0139, 2011.

Zhao, T., Shi, J., Lv, L., Xu, H., Chen, D., Cui, Q., Jackson, T. J., Yan, G., Jia, L., Chen, L., Zhao, K., Zheng, X., Zhao, L., Zheng, C., Ji, D., Xiong, C., Wang, T., Li, R., Pan, J., Wen, J., Yu, C., Zheng, Y., Jiang, L., Chai, L., Lu, H., Yao, P., Ma, J., Lv, H., Wu, J., Zhao, W., Yang, N., Guo, P., Li, Y., Hu, L., Geng, D., and Zhang, Z.: Soil moisture experiment in the Luan River supporting new satellite mission opportunities, Remote Sensing of Environment, 240, 111 680, https://doi.org/10.1016/j.rse.2020.111680, 2020.